MyWave

Report on Wave Coupling

Reference: MyWave-D1.4

Project N°: FP7-SPACE-2011-284455	**Work programme topic:** SPA.2011.1.5.03 – R&D to enhance future GMES applications in the Marine and Atmosphere areas
Start Date of project: 01.01-2012	**Duration**: 36 Months

WP leader: Peter Janssen **Issue:**

Contributors: Lucio Torrisi, Luigi Cavaleri, Korres G., Papadopoulos A., Varlas G., Katsafados P.

MyWave version scope: all project versions

Approval Date: **Approver:**

Dissemination level: Project

DOCUMENT VERIFICATION AND DISTRIBUTION LIST

	Name	Work Package	Date
Checked By:			
Distribution			
	Ø. Saetra (Project coordinator) Peter Janssen (WP1 leader) Luigi Cavaleri (WP1) Lucio Torrisi (WP1) Gerasimos Korres		

CHANGE RECORD

Issue	Date	§	Description of Change	Author	Checked By
0.1	25/10/14	all	First draft of document	Luigi Cavaleri, Paolo Pezzutto	Luigi Cavaleri
1.0	11/11/14	all	Document finalization	Luigi Cavaleri, Paolo Pezzutto	Luigi Cavaleri

TABLE OF CONTENTS

LIST OF FIGURES

GLOSSARY AND ABREVIATIONS

CNMCA	Centro Nazionale di Meteorologia e Climatologia Aeronautica (National Centre of Aeronautics Weather Science and Climatology)
HCMR	Hellenic Centre of Marine Research

APPLICABLE AND REFERENCE DOCUMENTS

Applicable Documents

	Ref	Title	Date / Issue
DA 1	MyWave-A1	MyWave: Annex I – “Description of Work”	September 2011

Reference Documents

	Ref	Title	Date / Issue

I INTRODUCTION

This deliverable concerns the coupling between two, meteorological and wave, models. One way (meteo to waves) coupling has been for a long while the norm, but Janssen (1989, 1991) showed that a two-way coupling, where the wave effect is transmitted back to the atmosphere, represents the correct physics, in so doing improving the results in also the meteorological model.

It has also been suggested that a two-way coupling would be more and more effective with increasing resolution. While the European Centre for Medium-Range Weather Forecasts (Reading, U.K.) has implemented the full coupling on a global scale since 1991, the matter has not received much attention at higher resolution, i.e. the local scale. In the MyWave project one of the targets was the implementation of a fully coupled system in the Mediterranean. Two actions have been taken in this respect, by the Italian Meteorological Service (henceforth CNMCA) together with the Institute of Marine Sciences (ISMAR), and by the Greek Hellenic Centre for Marine Research (HCMR). In the following pages the two systems, that use different meteorological models, are described. Given that the basic theory is the same, the two implementations are described in parallel, describing first the two backgrounds and the respective meteorological models. The wave model, WAM, is the same for both the systems. Then the respective test periods are described, each together with the related results. In the conclusion we summarize the overall results, also in the perspective of further developments.

II COUPLED MODEL ELEMENTS

II.1 COSMO and WAM (CNMCA)

II.1.1 The WAM Model

The global ocean WAve prediction Model called WAM was the first third generation wave model and it was conceived by the WAMDI group (WAMDI, 1988). WAM has as prognostic variable the two-dimensional wave spectrum from which diagnostic variables, such as significant wave height, average wave period and many other integral wave parameters can be deduced. The WAM model is used at the European Centre for Medium-Range Weather Forecasts (ECMWF, Reading, U.K.) as the operational wave model. It is tightly coupled to the local IFS (Integrated Forecasting System, ECMWF, 2012). To have a local modelling environment that conforms to the one at the Centre, in our work we have followed closely the theoretical basis established at the Centre by Peter Janssen (1989, 1991).

In particular the WAM model solves the Wave Action Equation (hereinafter WAE) based on the work of Klaus Hasselman (Hasselmann, 1961). The WAE describes the evolution of random waves in terms of the two-dimensional wave spectrum taking into account the influence of slowly varying media.

$$\underbrace{\frac{\partial}{\partial t}N}_{\text{Change in Time}} + \underbrace{\nabla_{\mathrm{X}}\left(\dot{\boldsymbol{X}}N\right)}_{\text{Advection in horizontal space}} + \underbrace{\frac{\partial}{\partial\sigma}\left(\dot{\theta}N\right)+\frac{\partial}{\partial\theta}\left(\dot{\sigma}N\right)}_{\text{Advection in spectral space}} = \underbrace{S_{tot}}_{\text{Total Source Term}} \qquad (1)$$

where the wave action is defined as the conserved quantity in slowly varying environment according to Bretherton and Garrtet (1969) as:

$$N_{(t,\mathrm{X},\sigma,\theta)} = \frac{E_{(t,\mathrm{X},\sigma,\theta)}}{\sigma} \qquad (2)$$

The advection velocities in the different phase spaces can be defined by the following equations (e.g. Keller, 1958).

$$\begin{aligned}\dot{\boldsymbol{X}} &= \boldsymbol{c}_{\boldsymbol{X}} = \frac{d\boldsymbol{X}}{dt} = \frac{d\omega}{dk} = \boldsymbol{c}_{\boldsymbol{g}} + \boldsymbol{U}_A \\ \dot{\theta} &= c_\theta = \frac{1}{k}\frac{\partial\sigma}{\partial d}\frac{\partial d}{\partial m} + \boldsymbol{k}\cdot\frac{\partial \boldsymbol{U}_A}{\partial s} \\ \dot{\sigma} &= c_\sigma = \frac{\partial\sigma}{\partial d}\left(\frac{\partial d}{\partial t} + \boldsymbol{U}_A\cdot\nabla_{\boldsymbol{X}} d\right) - c_g\boldsymbol{k}\frac{\partial \boldsymbol{U}_A}{\partial s}\end{aligned} \qquad (3)$$

which close the adiabatic part of the WAE. The right hand side of the WAE describes the physics of growth (S_{in}), decay (S_{ds}) and resonant non-linear interactions (S_{nl4}) among the different random waves within the discrete wave spectra as well as the near-resonant interactions (S_{nl3}) and the dissipative processes in shallow waters such as bottom friction (S_{bf}) and wave breaking (S_{ds}).

$$\frac{dN}{dt} = S_{total} = S_{in} + S_{nl4} + S_{ds} + S_{nl3} + S_{br} + S_{bf} \qquad (4)$$

The most important constituents for the coupling of waves to the atmosphere are the wind input term S_{in}, the white-capping dissipation S_{ds}, and the resonant non-linear interactions in deep water. These source functions govern the distribution of wave action within the discrete wave spectra and in so doing the apparent roughness of the ocean surface, which is the clearly defined interface between the ocean and the atmosphere. At the present stage of our long term plan we focus on the effect of the

surface roughness defined by the ocean waves and we neglect the thermodynamic part of the atmospheric model that of course also depends on the sea state. Further dependence on the ocean circulation and the thermodynamic balance of the ocean will be redefined in the next phase of our plan. There we will consider the influence of the waves on the ocean circulation, the fluxes of water vapour, the influence of spray formation from the ocean surface towards the atmosphere, and the generation of turbulence in the oceanic surface layer by the breaking of waves.

II.1.2 The COSMO Model

The COSMO model solves the non-hydrostatic, fully compressible hydro-thermo-dynamical equations in advection form (Eq. 1a-1d).

$$\begin{aligned}
\rho\frac{d\mathbf{v}}{dt} &= -\nabla p + \rho\mathbf{g} - 2\boldsymbol{\Omega}\times(\rho\mathbf{v}) - \nabla\cdot\underline{\mathbf{t}} \\
\frac{d\rho}{dt} &= -\rho\nabla\cdot\mathbf{v} \\
\rho\frac{dq^x}{dt} &= -\nabla\cdot\mathbf{J}^x + I^x \\
\rho\frac{de}{dt} &= -p\nabla\cdot\mathbf{v} - \nabla\cdot(\mathbf{J}_e + \mathbf{R}) + \varepsilon.
\end{aligned} \qquad (5)$$

where x indicates the constituent of the mixing e.g. dry air (d), water vapour (v), liquid water (l) and frozen state (f). The other variables represent vectors if they are bold, scalars in the other case. The involved variables are defined as follows:

t	time
p	pressure
T	temperature
ρ^x	partial density of mixture constituent x
$\rho = \sum_x \rho^x$	total density of the air mixture
$q^x = \rho^x/\rho$	mass fraction (specific content) of constituent x
$v = \rho^{-1}$	specific volume
e	specific internal energy
$h = e + pv$	specific enthalpy
$\mathbf{v}$	barycentric velocity (relative to the rotating earth)
I^x	sources/sinks of constituent x
$\mathbf{J}^x$	diffusion flux of constituent x
$\mathbf{J}_e$	diffusion flux of internal energy (heat flux)
$\mathbf{R}$	flux density of solar and thermal radiation
$\underline{\mathbf{t}}$	stress tensor due to viscosity
$\varepsilon = -\underline{\mathbf{t}}\cdot\cdot\nabla\mathbf{v}$	kinetic energy dissipation due to viscosity
$\boldsymbol{\Omega}$	constant angular velocity of earth rotation
$\mathbf{g}$	apparent acceleration of gravity
$d/dt = \partial/\partial t + \mathbf{v}\cdot\nabla$	total (Lagrangian) time derivative operator
$\partial/\partial t$	local (Eulerian) time derivative operator
∇	gradient (Nabla) operator

The prognostic variables are the horizontal and vertical Cartesian wind components, temperature (t), pressure perturbation (p', deviation from the reference state), specific humidity (q_v) and specific cloud water content (q_c); optionally: cloud ice content (q_i), specific water content of rain (q_r), snow (q_s) and graupel (q_g), the turbulent kinetic energy (tke). From these results several diagnostic variables are computed, which include the 2 metre temperature, the 10 metre wind speed, the maximum wind gusts at 10 metre height, the precipitation fluxes of rain and snow and others.

COSMO uses a rotated geographical (lat/lon) coordinate system horizontally and a generalized terrain-following height-coordinate with user defined grid stretching in the vertical. The numerical grid

is based on an Arakawa C-grid, Lorenz vertical grid staggering and it uses second-order finite differences for the spatial discretization, offering also options for up to 6th order horizontal discretization, where the default is a 5th order horizontal discretization. The default time integration scheme is the 2nd and 3rd order Runge-Kutta integrator according to (Wicker and Skamarock, 2002), but also a TVD 3rd order variant of it, where there are also some other possibilities available. Numerical smoothing may be applied using 4th-order linear horizontal diffusion with option for a monotonic version including an orographic limiter, where also other options are available.

II.2 POSEIDON/Eta and WAM (HCMR)

During the period M0->M0+18 of the project, a two-way coupled system for simulating the atmospheric and sea-state conditions over the Mediterranean and Black Seas have been developed. The coupled system consists of two components: the atmospheric model of the Greek POSEIDON monitoring and forecasting system (Papadopoulos et al., 2002; Janjic, 2001; Nickovic et al., 2001; Mesinger et al. 1988) and the WAM Cycle 4 wave model parallelized using OpenMP directives (Monbaliu et al., 2000; Korres et al. 2010).

The atmospheric model used is based on the latest version of the SKIRON/Eta mesoscale meteorological model which is a modified version of the Eta/NCEP model (Kallos et al. 1997, Papadopoulos et al. 2002). This version became the core of the second generation POSEIDON weather forecasting system (Papadopoulos and Katsafados 2009) and is fully parallelized to run efficiently on any parallel computer platform. It uses a two-dimensional scheme for partitioning grid-point space to Message Passing Interface (MPI) tasks. MPI is a protocol for the data exchange and synchronization between the executing tasks of a parallel job. The Eta model is designed to use either the hydrostatic approximation or the non-hydrostatic correction in order to be able to resolve high resolution atmospheric processes. For the specific application special care was taken in the estimation of the near surface wind speed, the friction velocity and the roughness. The application of the Monin-Obukhov similarity theory and the introduction of a viscous sub-layer permit the realistic estimation of the surface parameters.

The ocean wave component is based on the WAM Cycle-4 code written with OMP directives. In order to reduce unrealistic energy loss at boundary points in cases where the waves propagate parallel and near the coast we followed the technique of Monbaliu et al. (2000) where an alternative octant propagation coordinate system was introduced in the original WAM model code. For the octant advection scheme, eight propagation directions are defined instead of four in the quadrant scheme. The model uses 24 directional bins (15° directional resolution) and 30 frequency bins (ranging between 0.05Hz and 0.793Hz) to represent the wave spectra distribution. The model runs in shallow water mode without depth or current refraction (Korres et al. 2011).

III PHYSICAL BACKGROUND

III.1 CNMCA

The interaction of the atmosphere with the ocean surface is a fascinating and fast evolving field of physical oceanography and meteorology. Following the pioneering work of Phillips (1957) and Miles (1957), the quasi-linear theory of wave-atmosphere interactions, introduced by Peter Janssen (1989, 1991), is the one that is presently used in most of the operational wave forecasting systems worldwide. The basic assumption of Janssen's theory is that even for a young wind-sea the assumption of a logarithmic velocity profile in the atmospheric boundary layer is appropriate. Observational evidence over ocean conditions (Hristov et al., 2003), but also during strongly forced growth conditions (Troitskaya et al., 2012), underlines the validity of the quasi-linear assumption made in Janssen's theory. The formulation of the wind input source terms is:

$$S_{(\sigma,\theta),in} = \gamma \cdot N_{(\sigma,\theta)} \tag{6}$$

where

$$\gamma = \omega \varepsilon \beta x^2 \tag{7}$$

with

$$x = \left(\frac{u_*}{c}\right)\cos\left(\theta - \phi\right) \tag{8}$$

$$\beta = \frac{\beta_m}{\kappa^2}\mu \ln^4\left(\mu\right), \mu \le 1 \tag{9}$$

$$\mu = \left(\frac{u_*}{\kappa c}\right)\Omega_m e^{\frac{\kappa}{x}} \tag{10}$$

and

$$\Omega_m = \frac{g z_0}{u_*^2} \tag{11}$$

Here $\mathbf{u_*}$ is the friction velocity, **c** the phase velocity, **Φ** the wind direction at 10m height and Θ the discrete wave direction of the considered wave packet. $\mathbf{\Omega_m}$ illustrates that the growth rate depends on the roughness, which inherently depends on the sea state and this justifies the tight coupling between the surface wave model and the atmosphere. $\mathbf{\Omega_m}$ (eq.11) is defined as the Charnock coefficient divided by the friction velocity. The formulation is closed by defining the kinematic stress (total stress) according to Janssen (1991) as

$$\tau = \left[\frac{\kappa U_{(z_{obs})}}{\ln\left(\frac{z_{obs}}{z_0}\right)}\right]^2 \tag{12}$$

where the apparent roughness length is defined as

$$z_0 = \left(\frac{\hat{\alpha}\tau}{g\sqrt{1-\frac{\tau_w}{\tau}}} \right) \qquad (13)$$

with the wave-induced stress given by

$$\tau_w = \varepsilon^{-1} g \int_0^{2\pi} \int_0^{\infty} \gamma N_{(\sigma,\theta)} k d\omega d\theta \qquad (14)$$

It is important to note that beyond the discrete integration range, the prognostic part of the spectral wave model, a diagnostic σ^{-5} tail is assumed in order to account for the high frequency contribution to the wave induced stress that cannot be neglected.

The dissipation function must carefully balance the wind-input, especially in the high frequency part of the wave spectra, in order that the kinematic stress of well-known measurements (e.g. HEXOS, Katsaros et al., 1987) can be reproduced. It was found that the originally proposed formulation of Hasselmann (1974) needs to be modified in order to have realistic friction velocity estimates. Especially the high frequency part of the wave spectra was shown to be crucial in order to achieve this. For details about this consult Komen et al. (1994) and for the latest parameterization of these source terms see Bidlot et al. (2005).

The Charnock coefficient that is computed in the above given way is passed to the atmospheric model, which then adjust based on its own turbulence scheme to the new roughness regime provided by the wave model. Clearly there is inconsistency in the parameterization of the boundary layer in the wave model and the atmospheric model, we accept here both parameterizations of each the models but we introduce a new degree of freedom by a physical description of the surface roughness over the ocean. The replacement of the friction velocity of the atmosphere with the friction velocity coming from the boundary layer model of the waves would completely overwrite the turbulence model of the atmospheric part, which is not the intension of this work. The chosen procedure is very similar to what is done at the ECMWF in their coupled IFS model.

III.2 HCMR

In the offline coupled mode, the atmospheric model parameterizes the air-sea momentum by applying a viscous sub-layer scheme (Janjic, 1994) in which, the roughness z_0 over the sea surface is estimated according to the formula:

$$z_0 = \frac{a_w \cdot u_*^2}{g} \qquad (15)$$

In (15) the Charnock coefficient a_w, is kept constant (a_w=*0.018*) throughout the simulation. The ocean-wave model receives the near surface (10 m) wind components without any interaction between the two models.

However, the WAM model includes a set of diagnostic equations for modeling the sea surface roughness feedback on the near surface atmospheric boundary layer (Janssen, 1991). The spatial and temporal variability of the Charnock coefficient is estimated at each WAM time-step by

$$a_w = \frac{0.01}{\sqrt{1-\tau_w/\tau}} \qquad (16)$$

In (16) τ_w is the wave induced stress given by

$$\tau_w = \rho_w g \int \frac{k}{\omega} \cdot S_{in} \cdot d\omega d\theta \qquad (17)$$

The wave induced stress is mainly determined by the high frequency part of the wave spectrum consisting of the waves that have the largest growth rate due to the wind. In (17) ρ_w is the density of sea water, g is the gravitational acceleration, S_{in} represents the wind input term in the wave model, ω is the angular frequency, θ is the propagation direction and κ is the wavenumber. The total stress τ is estimated as

$$\tau = \rho_a \cdot C_D \cdot U_{ref}{}^2 \qquad (18)$$

where ρ_a is the density of air, U_{ref} is the wind speed at a reference height and C_D is the drag coefficient equals to

$$C_D = \left(\frac{\kappa}{\log(z_{ref} / z_0)} \right)^2 \qquad (19)$$

with κ being the von Karman constant. Combining (18) and (19) the total stress is given by

$$\tau = \left(\frac{\kappa \cdot U_{ref}}{\log(z_{ref} / z_0)} \right)^2 \qquad (20)$$

The estimated sea surface roughness is

$$z_0 = \frac{0.01 \cdot \tau}{\rho_a \cdot g \cdot \sqrt{1 - \tau_w / \tau}} \qquad (21)$$

Finally, the computed friction velocity

$$u_* = \sqrt{\tau / \rho_a} \qquad (22)$$

is applied in the wind input source function S_{in}.

In the fully coupled mode, WAM provides the atmospheric model with consistent values of Charnock coefficient, roughness and the friction velocity at each time-step. The atmospheric model applies the variable Charnock coefficient a_w in the formulation (15) for the estimation of the sea surface roughness length. According to the Mellor-Yamada-Janjic (MYJ) surface layer parameterization scheme (Janjic, 1994), a viscous sub-layer is assumed over the sea surface and operates under three sea state regimes: (i) smooth and transitional, (ii) rough, and (iii) rough with spray, depending on the roughness Reynolds number and finally on the friction velocity which is a monotonic function of R_r

$$R_r = \frac{z_0 u_*}{\nu} \qquad (23)$$

where $\nu = 1.5 \cdot 10^{-5}\ m^2 s^{-1}$ is the kinematic viscosity of the air (Figure III.1). The estimated friction velocity from WAM is then applied for the determination of the sea state regimes, instead of the friction velocity that is computed by the atmospheric model. In particular, the changes of the regimes have been adapted to $u_{*r} = 0.125\ ms^{-1}$ and $u_{*s} = 0.7\ ms^{-1}$.

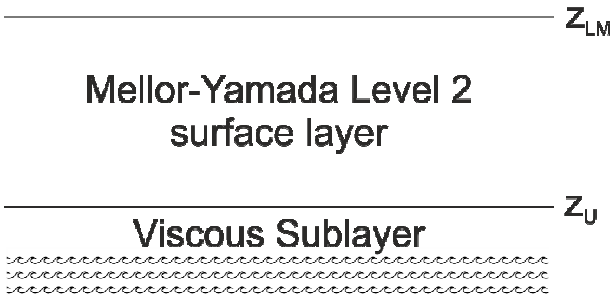

Figure III.1: The Mellor-Yamada surface layer with the viscous sub-layer over the ocean. The symbol ZLM is the height of the lowest model layer and ZU is the depth of the viscous sublayer for momentum. (Reproduced from Janjic, 1994).

The friction velocity of the atmospheric model is then estimated by

$$u_* = \left[\left(\frac{K_{Msfc}}{\Delta z_e} \right) (U_{LM} - U_{Z_U}) \right]^{1/2} \qquad (24)$$

where K_{Msfc} is the Mellor-Yamada level 2 discrete momentum exchange coefficient, Δz_e is the equivalent height of the lowest model level with the presence of the "dynamical turbulence layer" at the bottom of the surface layer. The final term is the scalar difference between the wind velocity estimated at the lowest model level and the velocity at a height z above the surface where the molecular diffusivities are still dominant (usually at the height of the viscous sub-layer). The depth of the viscous sub-layer for the momentum is estimated by

$$z_U = \zeta \nu \frac{M \left(\frac{z_0 u_*}{\nu} \right)^{1/4}}{u_*} \qquad (25)$$

where $\zeta=0.50$ and M is depending on the sea state regime. For smooth regime, $M=35$, and when the flow ceases to be smooth, $M=10$.

IV COUPLING STRATEGY AND TOOLS

IV.1 4. The PGMCL - Parallel Geophysical Model Coupling Library (CNMCA)

The WAM model has been successfully coupled to the COSMO model using a novel coupling library, written in native FORTRAN, especially conceived to fit the needs of both the models with respect to the parallel framework prescribed by the implementations. These needs derive from the historical evolution of the WAM code developed at a time when the computer memories were very limited. However, the approach in the WAM model, although complicated, is very effective, and therefore the coupling library was especially designed to fit the way the domain decomposition is done in the WAM model, but keeping in mind that in the future ROMS will be coupled as well. Therefore we have formulated the code so that the decomposition technique used in ROMS can also be easily embedded in the developed coupling library.

The coupling between the WAM and the COSMO models has been suitably done to minimize the changes in both the models and in such a way that after the compilation only one executable is present. The compilation has been totally overhauled for both codes and scripts have been used to setup automatically the dependency lists and *makefiles* in the proper order. In this way the final code can be compiled in parallel, e.g. by invoking the "make –j XX" commands, where XX indicates the number of threads to be used during the compilation.

The code merging strategy we have developed can be applied to all the numerical source codes that are parallelized based on the MPI interface, which is the dominant parallelization framework in geophysics.

The main idea is that, when the merged program is run, the common MPI communicator is split in several MPI communicators. In practice, having N processors at disposal, we decompose them as:

$$N_{ocn} + N_{wav} + N_{atm} = N \qquad (26)$$

Computationally, this means to split the "**MPI_COMM_WORLD**" communicator into sub-communicators by using the "**MPI_COMM_SPLIT**" command.

Hence, after that each model is using a

- **OCN_COMM_WORLD**,
- **ATM_COMM_WORLD** and
- **WAV_COMM_WORLD**.

Each model is running separately and essentially indepently of the others one. That is the only difference is in the communicator which has been replaced from **MPI_COMM_WORLD** to the relevant one.

The initialization of the coupling is done in 4 steps. First, the grids and parallelization metrics of the models are exchanged. Then, the global interpolation matrices are computed. Then the local interpolation matrices are built. Finally, the asynchronous MPI types are built. The step that takes the most time is the computation of the interpolation matrix. If we compute the interpolation from **A** to **B** then the model **B** is computing the interpolation matrix which is then sent to **A**. The computation in **B** can be parallelized easily. The resulting matrix is also stored on disk as a netcdf file in order to be readily accessible at the next run of the model.

For each pairs of models **A** and **B** there is a coupling/exchange interval in which data is exchanged. That is we do not need a common time for all models. The coupling is done at instantaneous times

and provides instantaneous values of the fields, i.e. no averaging is done. In other words **A** and **B** are fully synchronized at the time when the exchange of information between certain models is required. It cannot be over emphasized that the above framework can hold as many models as desired, the only hurdle being that the models have to be called as subroutines within the framework of the coupling.

Each model is Depending on the value of the MPI_SPLIT either the WAM model or the COSMO model is run as the main routine. Using this approach combines both the pipe approach of limited modification to the code and the approach of full integration where every model becomes a subroutine. It also provides a useful way of abstraction since every model has its own communicator, which is one of the main benefits of the newly developed PGMCL library. However it should be pointed out that this procedure has the disadvantage that the minimal number of processors must equal the number of coupled models. However, this is a very minor problem because the multi-core architecture is now very common. Another issue is that the number of processors needs to be adjusted, i.e. we need to know which ones are more processor hungry. The method here is to experiment and to read the runtimes that indicate the time spent by the model waiting for others.

In order to continue the approach of minimal changes to each of the models, the grid of each model was not modified, see Figure IV.1 and Figure IV.2 respectively. It is important to remember that the requirements for a numerical grid of an atmospheric model are different from the ones of a wave model. Forcing the same grid for both the models would impose on them unnecessary, and almost impossible to realize, requirements. On the contrary the solution is to use linear interpolation. For some variables, as e.g. wind speed and direction, this is straightforward and can be done in a relatively simple way. Much more care is required for physical variables that can show substantial differences between land and sea. Obvious examples are humidity and air temperature. In this case, because we focus on the air-sea interactions, and if acting on the land-sea border, it is convenient to select only the wet points.

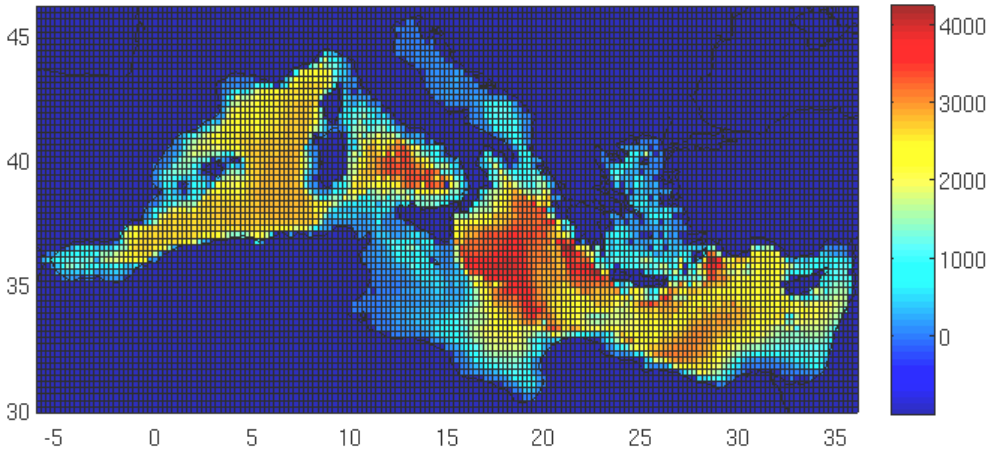

Figure IV.1: Grid of the WAM model with the bathymetry (in meters, according to color map) of the Mediterranean Sea.

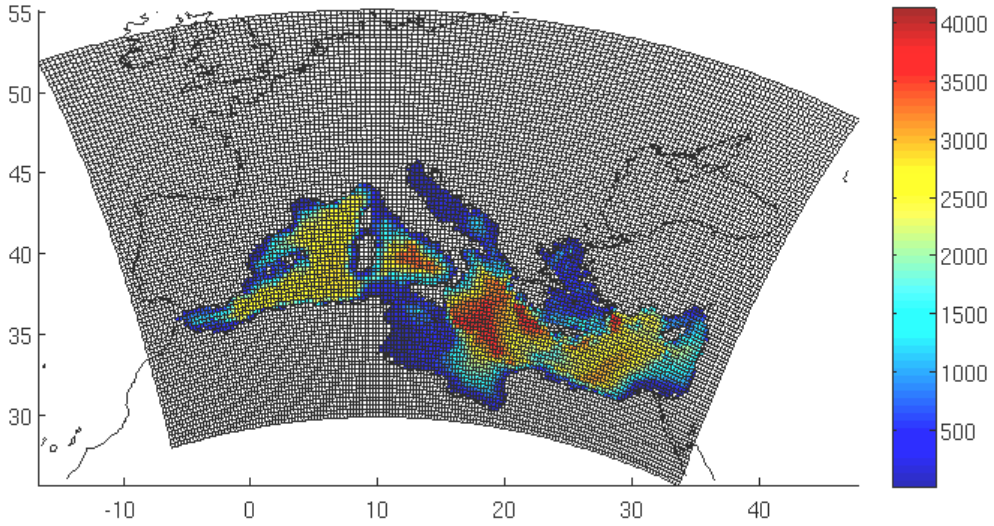

Figure IV.2: Bathymetry of the Mediterranean Sea interpolated from the WAM grid on the COSMO grid using the PGMCL coupling library

For the flow of information in the other direction, *i.e.* from the sea to the atmosphere, for each atmospheric point close to the land-sea border, out of the corresponding WAM grid points for interpolation we consider only the wet ones adapting accordingly their weight coefficients, eventually choosing the closest sea point.

This coupling strategy is very robust in terms of getting the right values at the right point. Should a more sophisticated interpolation method, as *krigging* or a higher order, be required, this could easily be introduced. For vectorial quantities, as wind, a previous transformation from the COSMO grid to the standard lat-lon system is required.

Once all the interpolation weights and the partition of the nodes are defined, then each node knows:

- what every other node has in its augmented domain (the domain + the ghost points)
- what every node needs for the interpolation,
- given this information the interpolation and exchange of data are executed in a single line of code that correspond to the send and receive commands of MPI.

The above formalism is near optimal in term of speed and allows efficient communication between all the models. It is also near optimal in the initialization part of the coupling. Note that with this configuration the communication is not a bottleneck for the coupling. What can be a bottleneck in term of speed is the relative speed of the models. Therefore it is convenient to find a proper load balancing on HPFC architectures, which can be done based on work estimates and achieved iteratively during runtime. This is computer dependent; hence the optimal solution must be defined for each specific application. During the development stage the results of the exchanged fields have been systematically checked in order to guarantee their consistency.

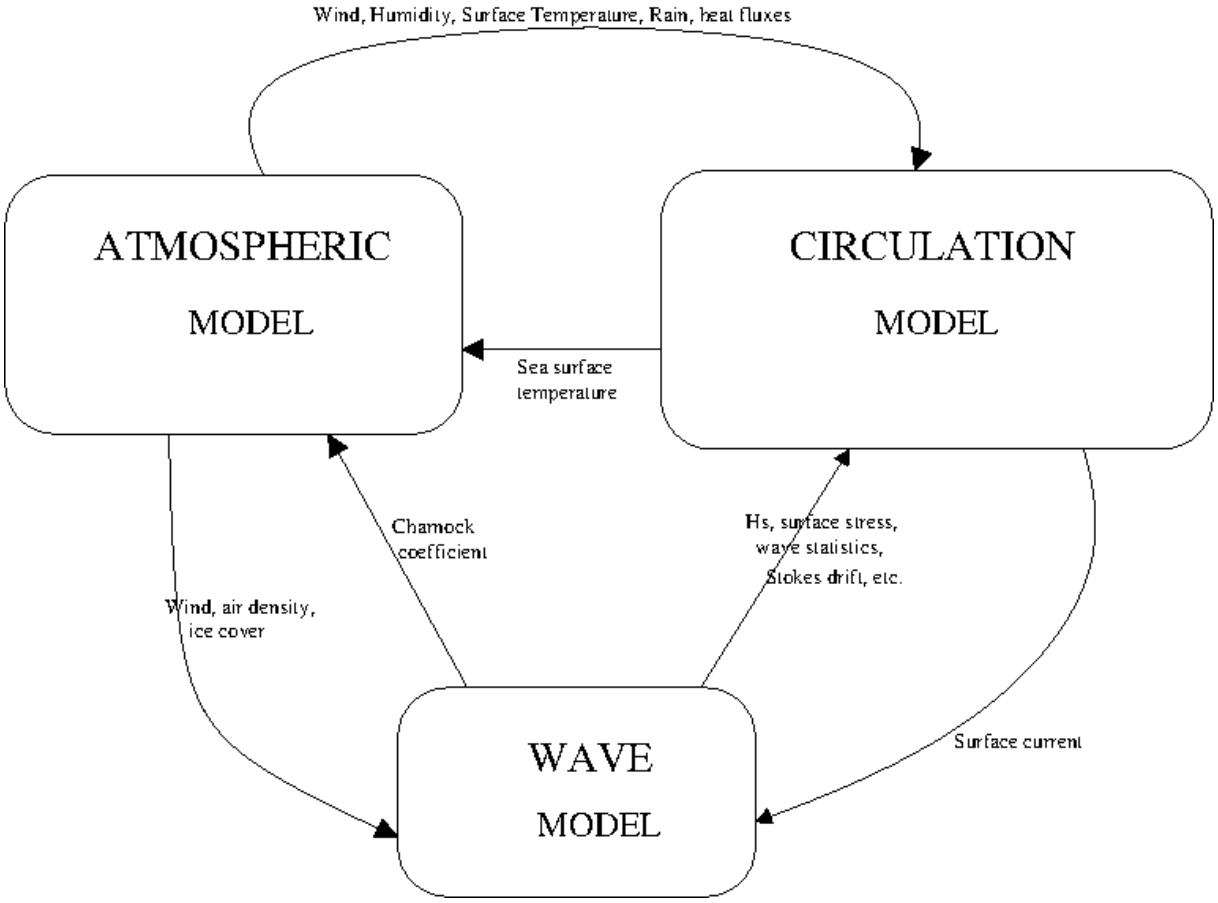

Figure IV.3: The exchange of the three way coupled COSMO-WAM-ROMS models

As already mentioned, our interest is on the Mediterranean Sea (see Figure 1). As is the common practice in Atmospheric modeling, one needs to put the boundary far away from the Mediterranean Sea. We ensure that the grid of the WAM and ROMS model is strictly contained into the grid of the COSMO model. Since the COSMO grid has been extended to a larger region than the Mediterranean for providing the high resolution modeling, the WAM and ROMS fields are not available over the Atlantic Ocean. Therefore, we choose the following modelization: When the WAM fields are available then we use them, otherwise we use the standard modelization of COSMO.

This kind of strategy is intrinsic to the chosen modelization. All the models have to be able to run with the fields of the other models. However, when such are not available then they need to be able to provide reasonable results. When doing the coupling, both the models actually run in parallel and exchange data at predefined times. For the wave model this time is chosen at the end of the fractional step method after the surface stress has been recalculated. For the COSMO model this is in the middle of the integration itself, since the values are needed for the evaluation of the apparent roughness length z_0. The COSMO model sends to the WAM model the wind and the air density used to compute the waves. The WAM model sends back the Charnock parameter used in COSMO for the computation of the turbulence scheme. The ROMS model sends the currents to WAM and to COSMO. It also sends the Sea Surface Temperature to COSMO (see Figure IV.3).

The COSMO and the WAM model have been coupled using an innovative coupling procedure, especially designed to allow for the different structure of the two models and the decomposition of each numerical framework. The structure of the coupling is absolutely general, capable to accommodate other models in the overall coupling procedure. The general character of the approach limits the work required for the coupling (our procedure has just 3000 lines of code). However, care is required in when, during the numerical integration of each model, the information is to be transferred between the models. As an example, during our first trials, we found unrealistic large values of the Charnock coefficient, especially close to the land-sea border. This turned out to be due to passing the reciprocal information at the wrong time combined with an error in the interpolation areas across the land-sea border.

IV.2 Setting up the two-way atmosphere- ocean wave coupled system (HCMR)

The overall communication between the various POSEIDON forecasting system models is depicted in Figure IV.4. In POSEIDON, an offline coupling of the air-sea interaction processes has been established between the atmospheric, the ocean-wave and the ocean-circulation models. Within this scheme, the atmospheric model generates and sends the appropriate fields to the ocean-wave (10 m winds) and circulation models (10 m winds, heat and water fluxes) without any further interaction. Within MyWave project the interaction and communication between the atmospheric and the wave model components has been upgraded to a two-way fully coupled system.

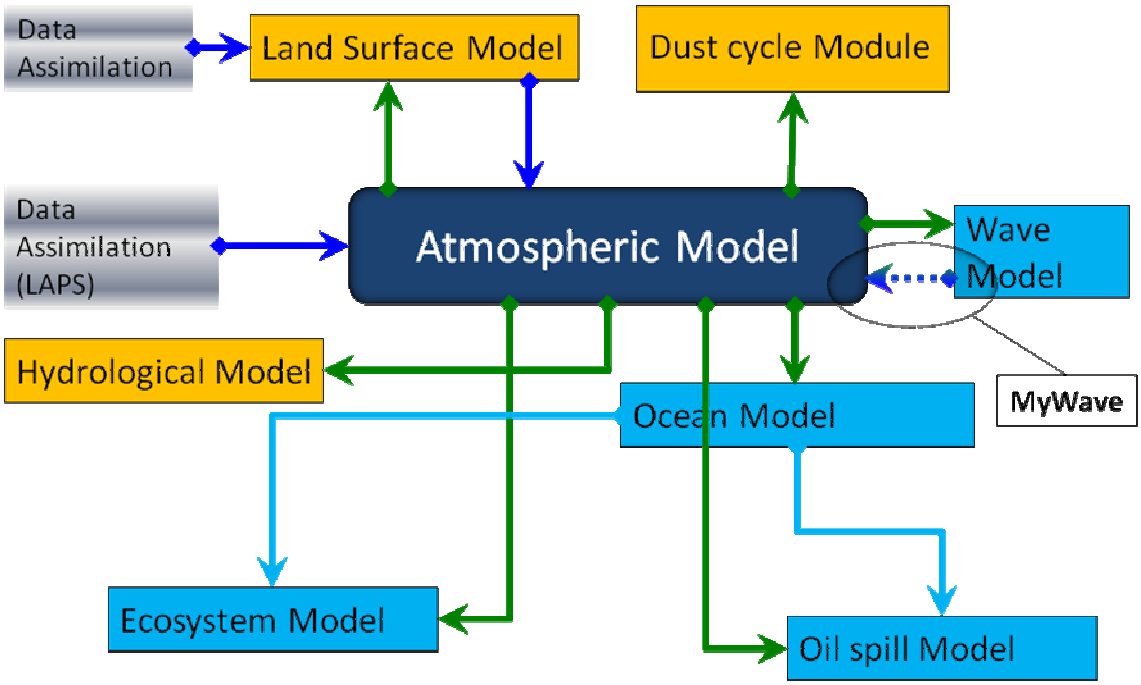

Figure IV.4: The operational chain of the POSEIDON system and the two-way coupling between the atmospheric and the ocean wave components.

The new system is called WEW and it is based on the Eta atmospheric model (atmospheric component) and the WAM Cycle 4 wave model (wave component). In the two-way coupled mode the Eta and WAM models utilize different domain projections, fundamental time integration, grid orientation and grid cell size. Therefore, a major effort has been devoted to synchronize and handle the two-way data exchange between the atmospheric and the ocean-wave components of the coupled system. These exchanges are built upon the **Message Passage Interface** (MPI) since it becomes a standard for developing applications under parallel environments. Under the parallel procedure of Multiple Program Multiple Data (MPMD), the two components are carried out as parallel tasks on different processors and they exchange information in a direct way. Thus, the parallel execution of the system is totally handled by the *mpirun*/*mpiexec* commands and the two components are keeping their own executables. The communication between the two models is practically done through *MPI_Send* and *MPI_Recv* calls every source time step of the wave model integration and the system runs flawlessly combining both MPICH and OMP environments (Figure IV.5).

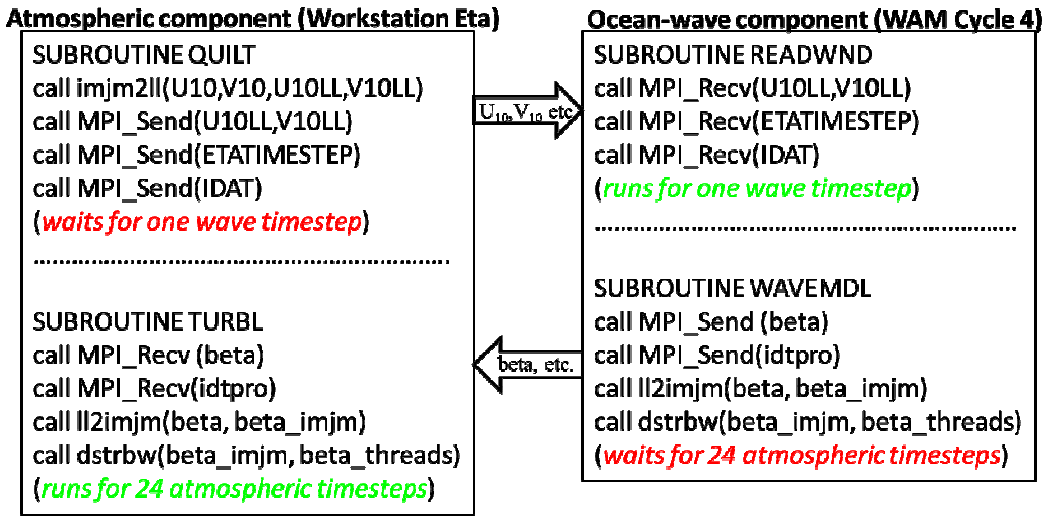

Figure IV.5: The WEW exchanges near surface U,V components and Charnock coefficient (beta) every time-step of the ocean-wave model.

During the initialization phase, the atmospheric model starts at first and loads the inter- and intra-communicators. The atmospheric model sends to the wave model the near surface wind components and receives the variable Charnock coefficient array, which is applied for the estimation of z_0 in the surface layer parameterization scheme. Each data exchange requires re-projection from the atmospheric model Arakawa-E grid to the ocean-wave model regular lat-lon grid and vice versa (Figure IV.6). For consistency, the sea-land masks are exchanged at the initialization stage and the atmospheric to ocean-wave time-steps ratio is currently defined as *1/24* but it can be easily adjusted to any other configuration through the main *namelist* of the system. Moreover, data exchanges can be easily expanded or cut off and the ocean-wave outputs (significant wave height and period, Charnock coefficient, friction velocity, etc.) are finally redirected through the internal communicators as outputs of the atmospheric component.

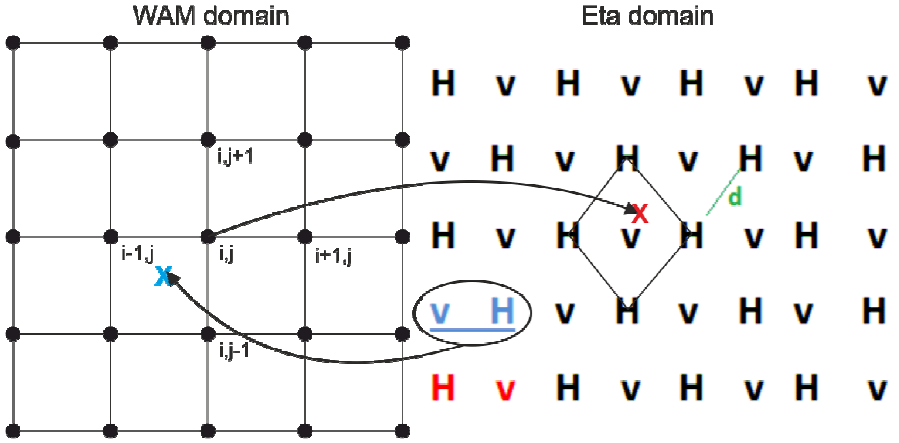

Figure IV.6: Sketch of the WEW multi-grid structure. The transformations from the Arakawa-E grid to the regular lat-lon grid and vice versa are also depicted.

The initial version (v0.1) of WEW ($1/10^o$ x $1/10^o$) was configured on a 2x2 topology for the atmospheric component (Figure IV.7) with two additional threads allocated for setting the I/O servers of the model. Another two threads were dedicated to the ocean-wave component being parallelized with OMP directives. The current version (v0.05) of the coupled system has been configured on a very fine horizontal resolution of 1/20°x1/20° with 493x461 E-grid points and 1001x381 regular lat-lon points. Numerous tests have been performed in order to extract the optimum topology. To this end, 28 threads have been allocated in total, 20 dedicated to the execution of atmospheric component (4 of them are the I/O servers) and the rest 8 are reserved for the ocean-wave component. Currently, WEW is running on HCMR Intel Xeon platform cluster using in total 28 threads at 6 nodes but it is easily

portable in any other architecture and flexible to adopt a different topology. For this configuration WEW requires almost 10 minutes for each simulation hour.

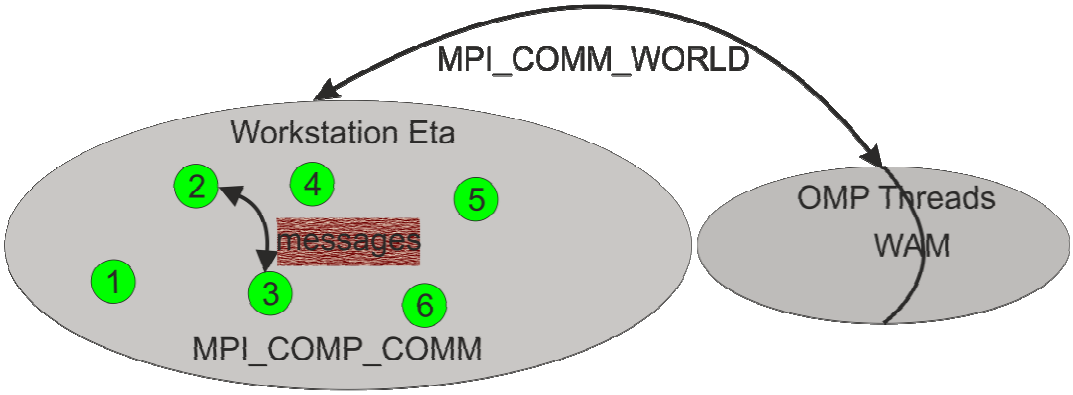

Figure IV.7: The WEW intra- and inter-communicators (for WEW v0.1).

A multi-level flowchart of the system and data exchanges in both is depicted in Figure IV.8. In the offline coupling mode (CTRL hereafter) the atmospheric component sends hourly near surface wind velocity to the ocean-wave model avoiding any other interaction between the two models (red line). In the two-way fully coupled mode (WEW hereafter) the atmospheric model sends every time step the near surface (10m) wind components and receives various near sea surface variables. In more details, WAM at each time step provides the atmospheric model with consistent values of the Charnock coefficient field, friction velocity, total surface stress etc. The atmospheric model applies the variable parameters directly in the Mellor Yamada surface layer parameterization scheme for the next time step estimation of the near surface wind components and the accurate determination of the viscous sub-layer and the parameterization of the air-sea momentum fluxes.

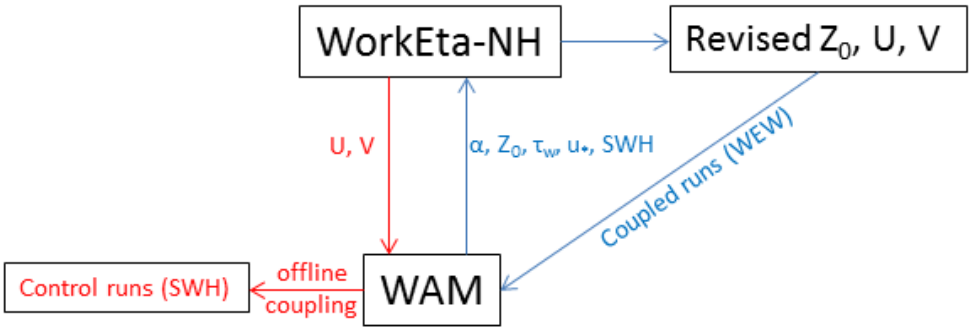

Figure IV.8: Informational flow for the offline coupled (red lines) and the two-way coupled simulations (blue lines).

V SYSTEM CONFIGURATIONS

V.1 CNMCA

The coupled model has been validated on a 0.25° grid for the waves and an equivalent grid for the atmosphere. The vertical representation of the atmospheric model is given by a logarithmically distributed grid with 40 vertical layers. The model time steps have been set to 300 sec for both the wave and the atmospheric model. The setup of the atmospheric model is, except the horizontal resolution, equivalent to the operational model setup of NETTUNO at CNMCA. The grid of the atmospheric model covers the region of Europe, whereas the grid of the wave model is focused on the Mediterranean Sea (see Figure V.1). The wave model is setup using 36 directions and 36 frequencies logarithmically distributed starting from 0.05Hz. The atmospheric model was forced at the boundary hourly using ECMWF

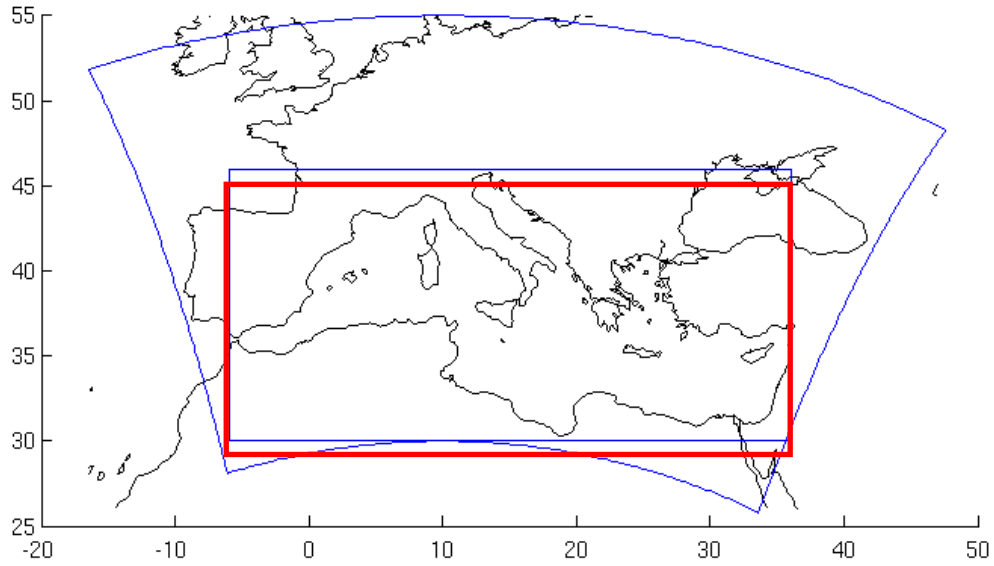

Figure V.1: Domains of the coupled model. The blue line indicates the COSMO domain. The red one indicates the WAM domain for the Mediterranean Sea

V.2 HCMR

The consistency and performance of WEW has been extensively tested within the MyWave project framework. Therefore, various simulations of preselected case studies have been contacted and the results have been statistically evaluated. The domain of model implementation encompasses the Mediterranean Sea and the Black Sea on a horizontal resolution 0.05°x0.05° (Figure V.2). During the initial stage of system development, a series of tests were performed on the coarser grid of 0.10°x10°. Gridded data from the European Centre for Medium range Weather Forecast (ECMWF) are used as initial and boundary conditions of the atmospheric model component. The grid of the wave model for the Mediterranean and Black Seas covers the geographical areas 8°W - 42°E to 29°N - 48° N as it is shown in Figure V.2 (black line) on a similar to the atmospheric component resolution. The different projections used by the model components yields a mismatch between the two domains. Thus, a constant Charnock coefficient is implemented for the sea grid points of the atmospheric domain being outside the wave model domain (western boundary of the atmospheric model for example).

Additionally, a 1-2-1 smoothing filter is also applied over the transition zone of the ocean-wave model domain to the atmospheric one in order to reduce any artificially generated waves.

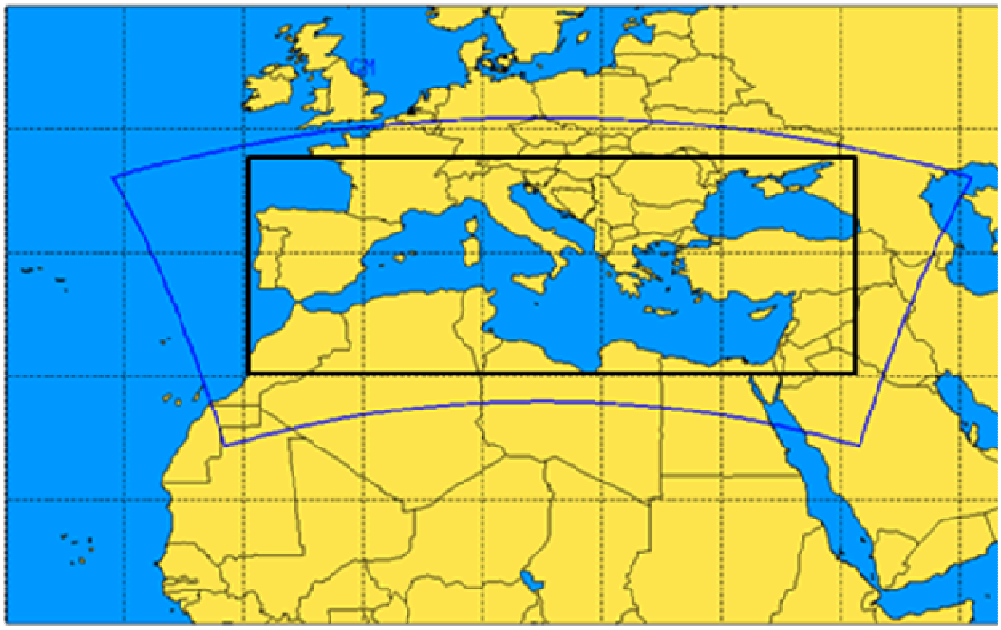

Figure V.2: Current domains configuration of the atmospheric (blue line) and the ocean-wave models (black line).

The initialization of WAM is based on a wind–sea spectrum computed on the basis of the initial wind field and it is produced during the pre-processing stage of the atmospheric model (cold start). The propagation time step is 120 sec while the source time step is set to 360 sec. Each component of WEW keeps its own time step while the coupling procedure exchanges data on the source time step of WAM, DT_w=360 sec. The relevant time step of the atmospheric model is DT_a=15 sec and the time step ratio between the two components is $N=DT_w/DT_a=24$. Thus, the exchanging procedure activates every 24 time steps of the atmospheric model. Every hour (3600 sec) WEW stores its unified outputs (including atmospheric and ocean-wave fields) on the native Arakawa-E grid. The configuration of the system is summarized in the Table V-1.

Table V-1: The configuration of the WEW current version (v0.05).

WEW v0.05	Atmospheric component	Ocean wave component
Integration domain	Mediterranean Sea, Europe, Black Sea	
Grid	Arakawa semi-staggered E grid defined in transformed lat/lon coordinate system	Regular lat/lon coordinate system
Horizontal grid increment	0.05°x0.05°	
Vertical coordinate	Step mountain, η coordinate	-
Vertical levels	38	-
Time steps (sec)	15	120/360
Initial & Boundary conditions	ECMWF, 0.5x0.5, 11 isobaric levels, 6hr update of the boundary conditions	Initialization from the atmospheric component, refresh rate every 360 sec
MPI/OMP topology	16 MPI processing threads + 4 I/O servers=20	8 OMP threads

VI VERIFICATION

VI.1 Validation of the Coupled Results (CNMCA)

VI.1.1 Qualitative Validation of the results

It is clear that a full validation of the described coupled system would require application for a long period and, most of all, coherently with operational use, continuous data assimilation. This would allow meaningful and significant comparison with measured data. In our case, both for the used resolution (0.25o) and for not using data assimilation for the initial condition for each forecast period, we can only look for a qualitative validation. Nevertheless, because we look for the significance and implications of coupling, the results are indicative for our present purpose.

We start the validation with a check of the distribution of the Charnock coefficient. Figure VI.1shows this distribution out of the two-day forecast of ECMWF. This is compared with the ones in Figure VI.2 (apologies for the different graphical system) showing the resulting distributions for the test period in the Mediterranean Sea, respectively with (left) and without (right) coupling. The experimental results match well, as range and distribution, the operational ones of ECMWF. Although the differences between the coupled and uncoupled runs are not very large, there are significant differences whose implications are clearer in the overall statistics.

The first quantitative comparison is between the corresponding (coupled vs uncoupled) 10 m wind speeds, surface atmospheric pressures and significant wave heights. Indeed, as expected, U_{10} and Hs are lower in the coupled runs, with also a more limited deepening of the developing low pressure systems. Figure VI.3 shows a comparison (scatter diagram) between the coupled and uncoupled significant wave heights. The best-fit line suggests a 5% difference between the two sets.

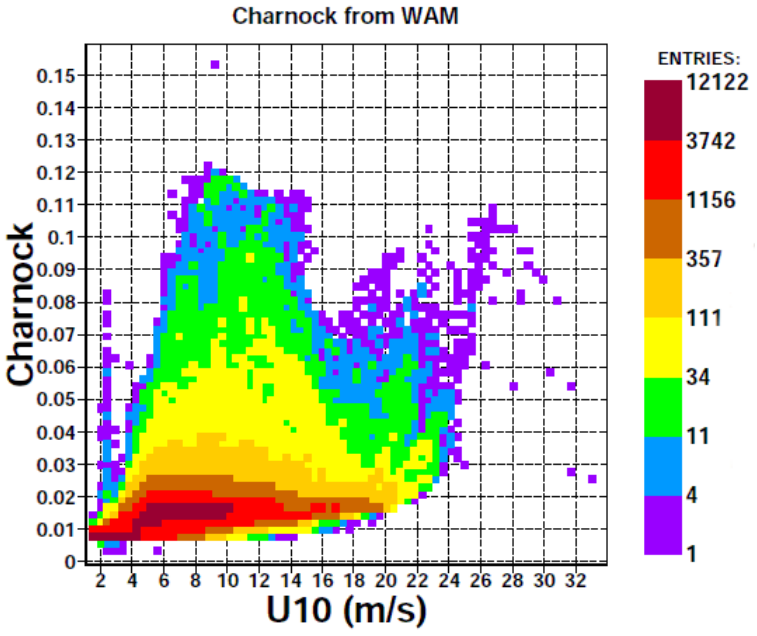

Figure VI.1: Charnock parameter versus wind speed. Distribution out of the two-day forecast of ECMWF distribution out of the two-day forecast of ECMWF.

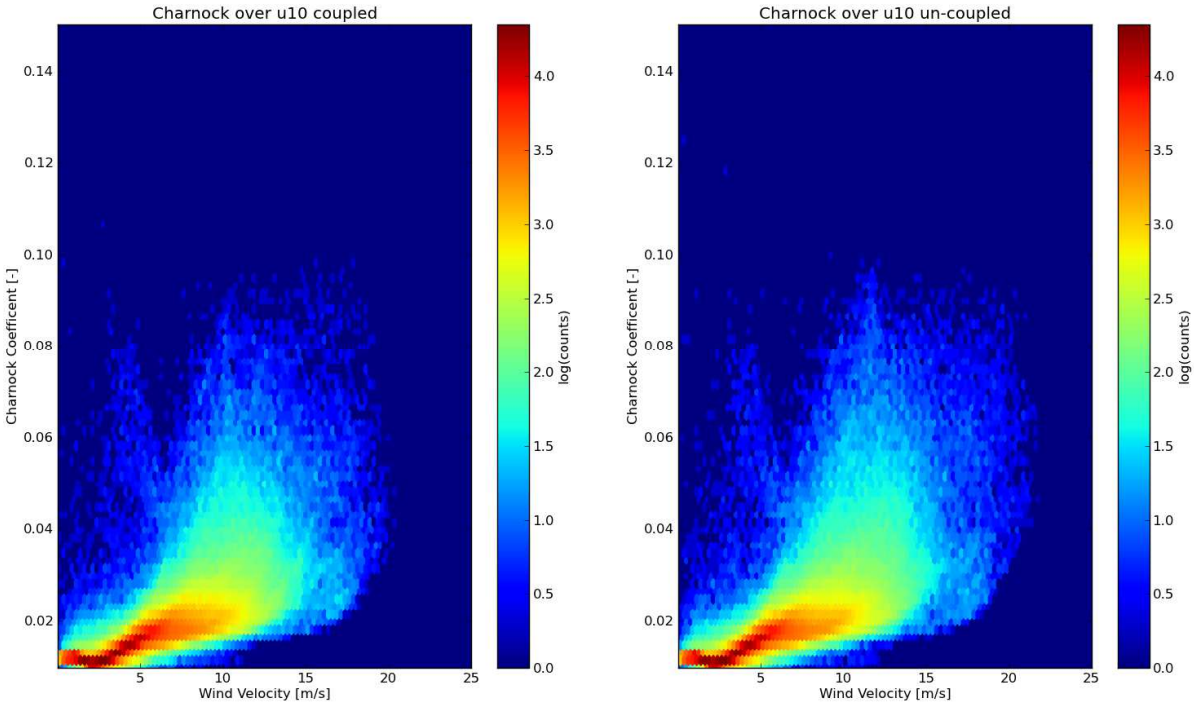

Figure VI.2: Charnock coefficient for the coupled (left) and the un-coupled (right) WAM run.

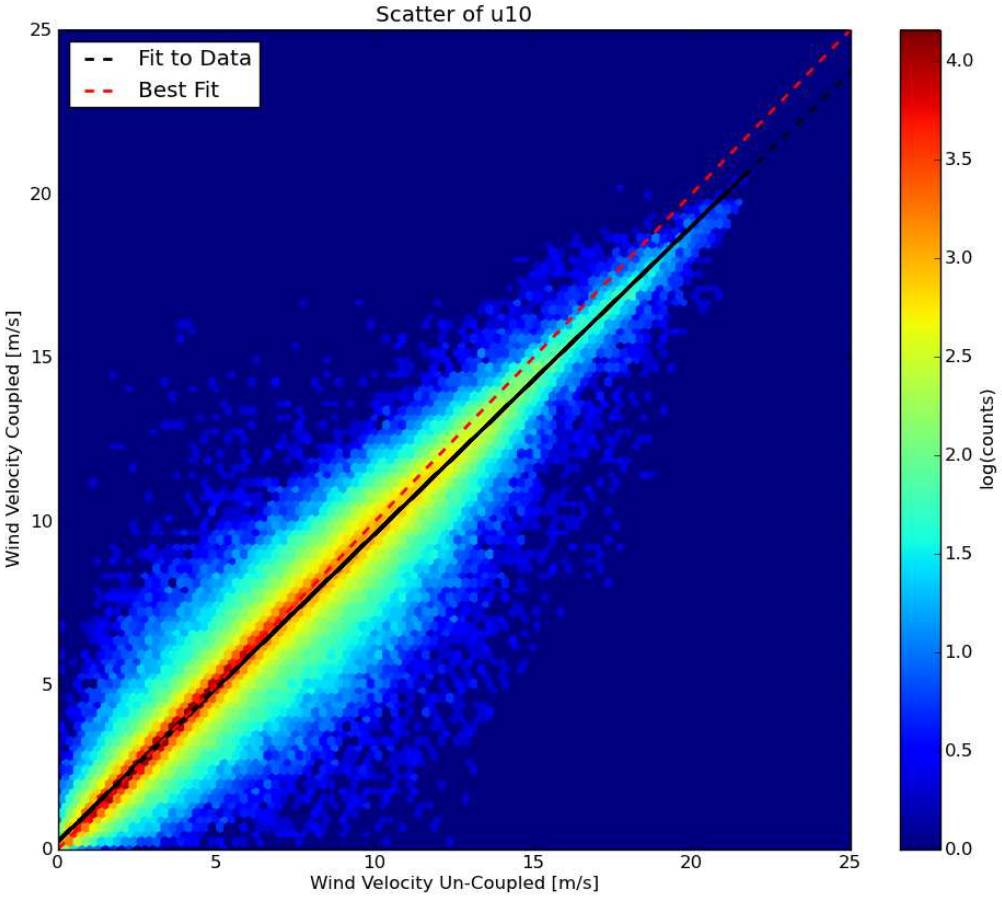

Figure VI.3: Scatter plot of the wind velocities of the coupled and uncoupled model run. Line of perfect fit is red; line of best fit is black.

An interesting example is offered by the development of a cyclone (at least in our non-assimilated runs) in the Eastern Mediterranean during another trial period. The intense development led to an active generation, hence to a strong air-sea interaction. As expected, there are evident differences in the H_S, U_{10} and pressure p fields (Figure VI.4). While the positive and negative differences in the middle panel indicate also a shift in the position of the minimum, the obvious negative differences (coupled minus uncoupled) of significant wave heights (lowest panel) point to the clear effect of a higher surface roughness in the actively generating area.

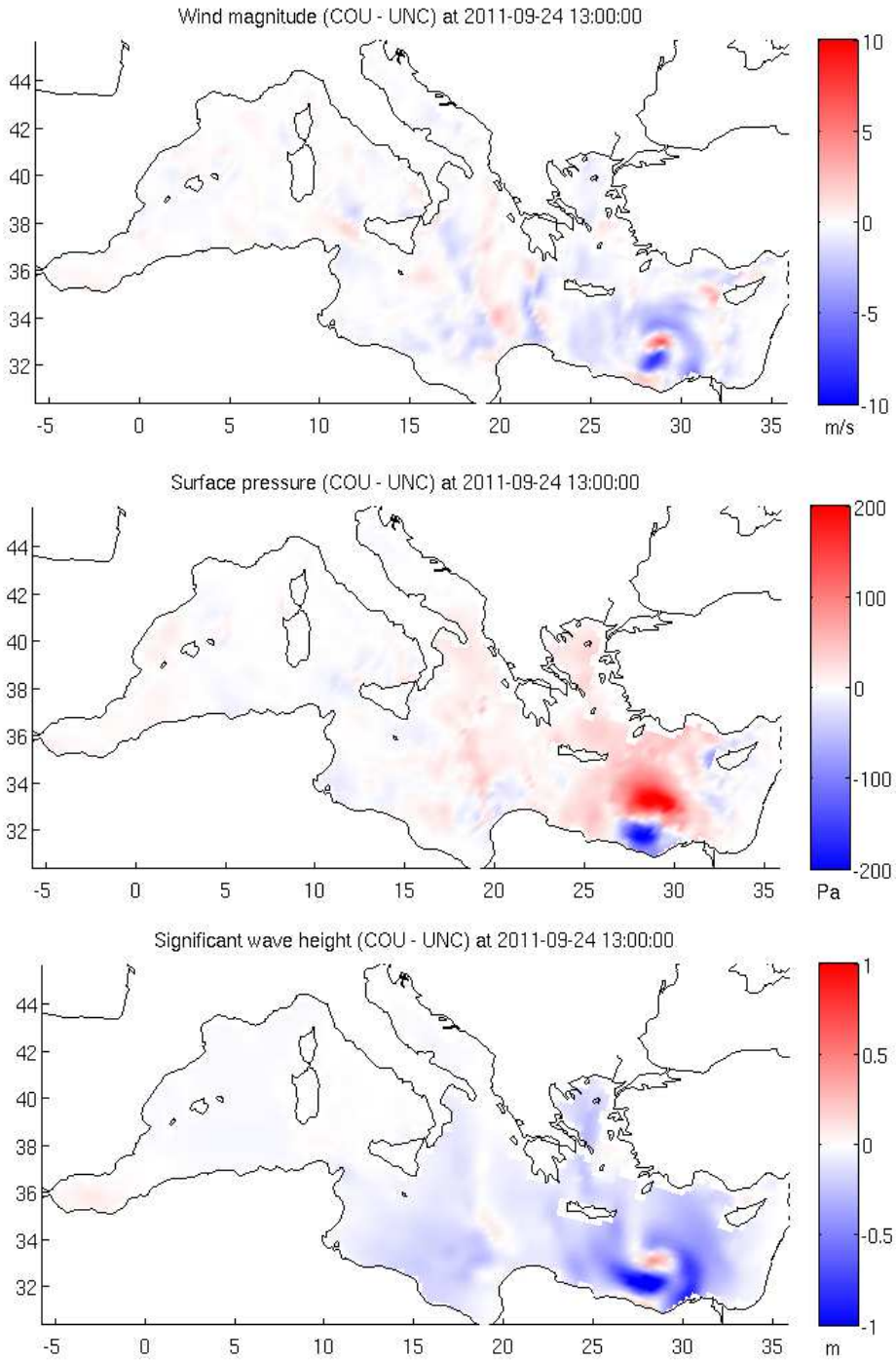

Figure VI.4: Difference in wind velocity [m/s], surface pressure [Pa] and significant wave height [m] during a cyclone in the Aegean Sea at the 24.9.2011 13:00.

Finally in the scatter diagrams (Figures V-5-11) and Tables V-1-6 we report the overall statistics concerning H_s and U_{10}, derived from the comparison with the corresponding measured data from the altimeters of the ENVISAT, Jason, Jason-2 and ERS-2 satellites. Each table, divided into different panels, report a) the overall (two months, Nov-Dec 2010) results for significant wave height for the

couple and uncoupled runs (the parameters are defined in the tables below), b) similar results for the wind speed, c) wave and wind essential statistics for the coupled case, and d) for the uncoupled one. The last two statistics, c) and d), are provided for single ten-day periods to make evident the progressive deterioration of the results (bias, RMSE) with time passing, i.e. while we move towards the winter and more stormy season. The last decease of the year is a notable exception.

For our immediate interests, i.e. of comparing the coupled vs. the uncoupled runs, there is a clear, almost uniformly distributed, tendency for lower differences and parameter values in the coupled case. In particular the bias, out of an average 1.65 m Hs altimeter value, is reduced of almost 50% and the scatter index of 20%. The corresponding values for U10 are 48% and 5%.

Based on these results that have been obtained without any tuning of the each of the coupled models, it is clear that taking into account the waves in the atmospheric boundary layer is a 1st order correction of the physics in the coupled system. The models have been tested and shown to be stable and robust. Their validation has shown that the most important parameters are in the expected range. Also the qualitative validation of the coupled model is giving the anticipated effect on the atmospheric boundary layer as well as for the surface wave model. The effect of the coupling of COSMO to WAM results for a young and growing wind sea in an increased apparent roughness length coming along with reduced wind velocities that are compensated with increased pressure, which reduces the pressure gradients in cyclonic wind fields as it is anticipated. Although their significance is partly limited by running the experiments without data assimilation (the system is driven only by the assimilated boundary conditions from the IFS), the extended comparison with multiple altimeter significant wave heights and wind speeds strongly suggest that the coupling leads to a substantial reduction of errors.

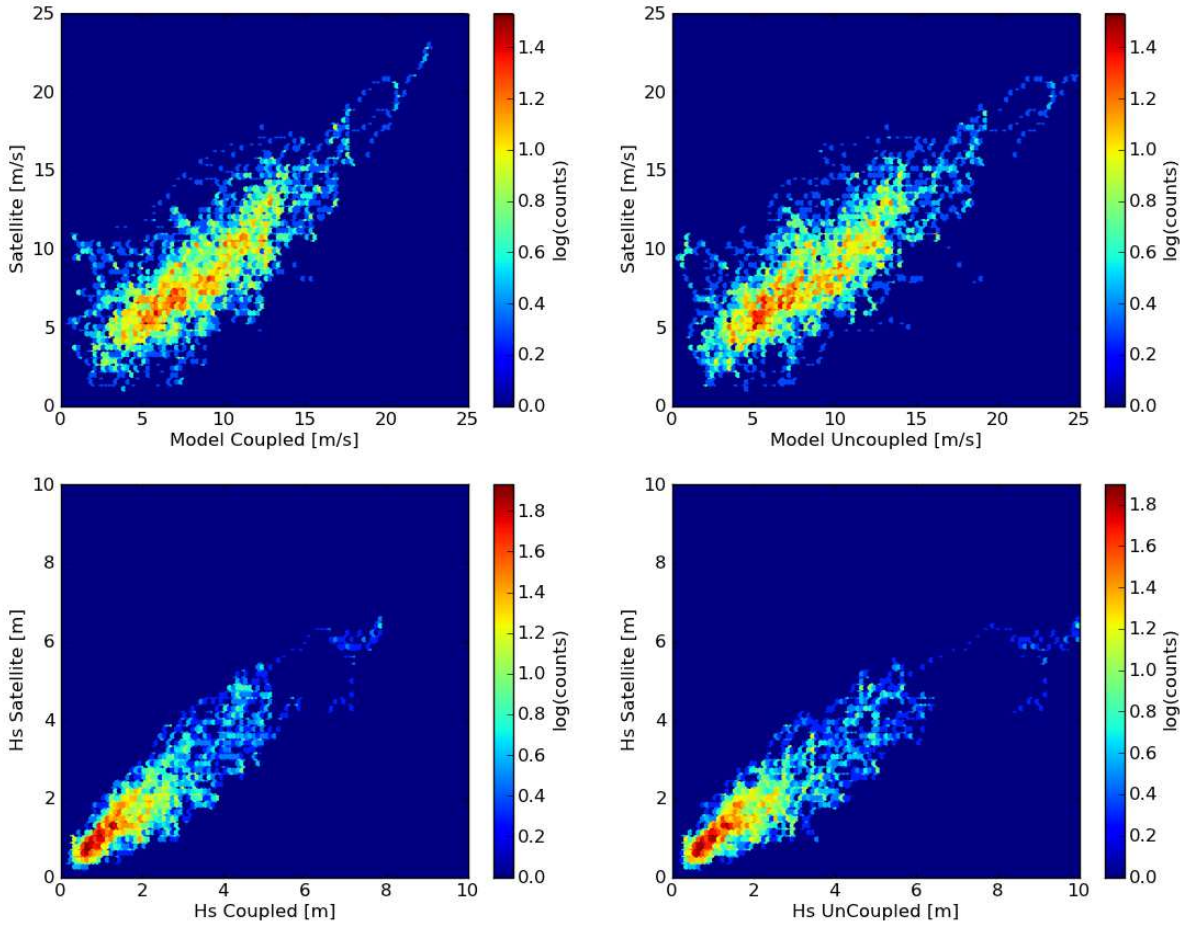

Figure VI.5: Comparison of winds and waves for Jason-1.

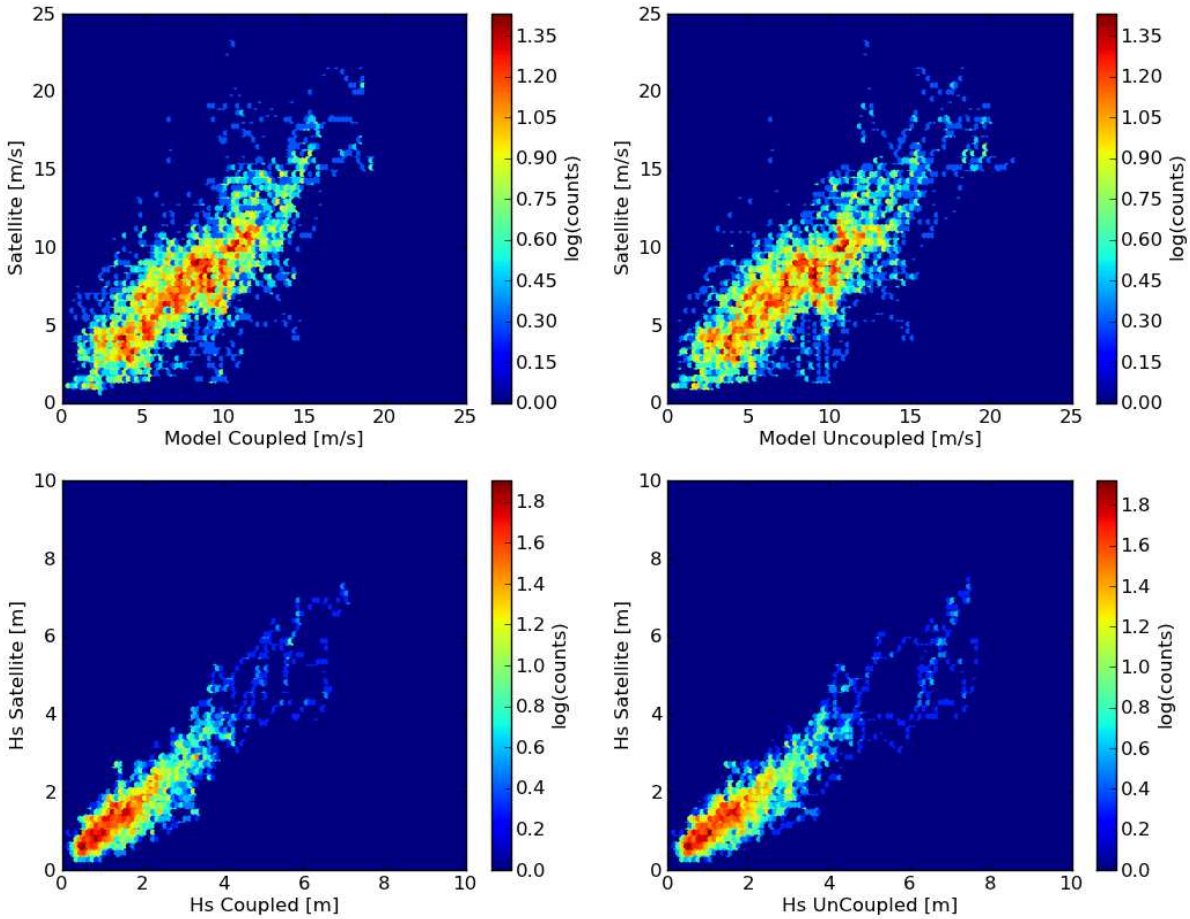

Figure VI.6: Comparison of winds and waves for Jason-2.

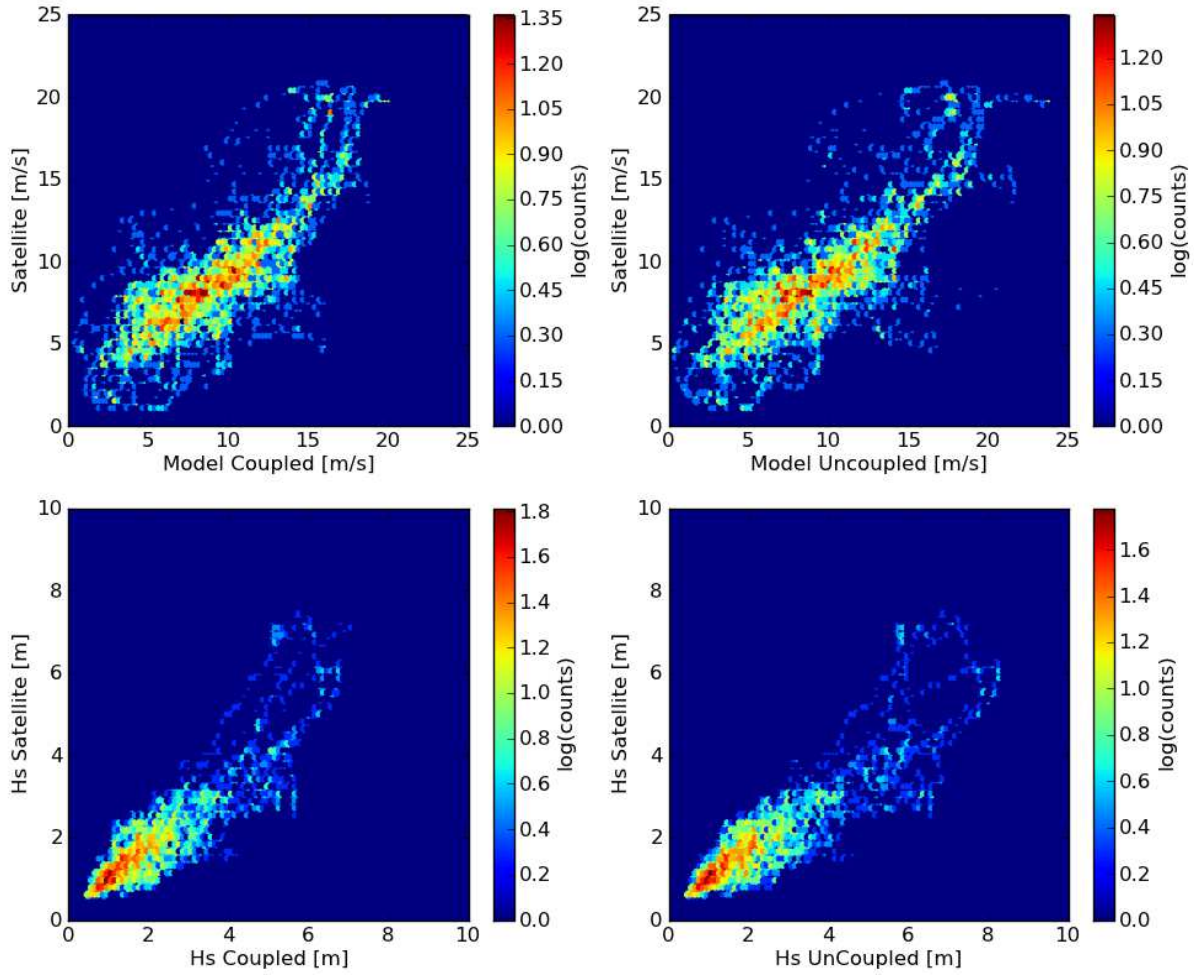

Figure VI.7: Comparison of winds and waves for ENVISAT.

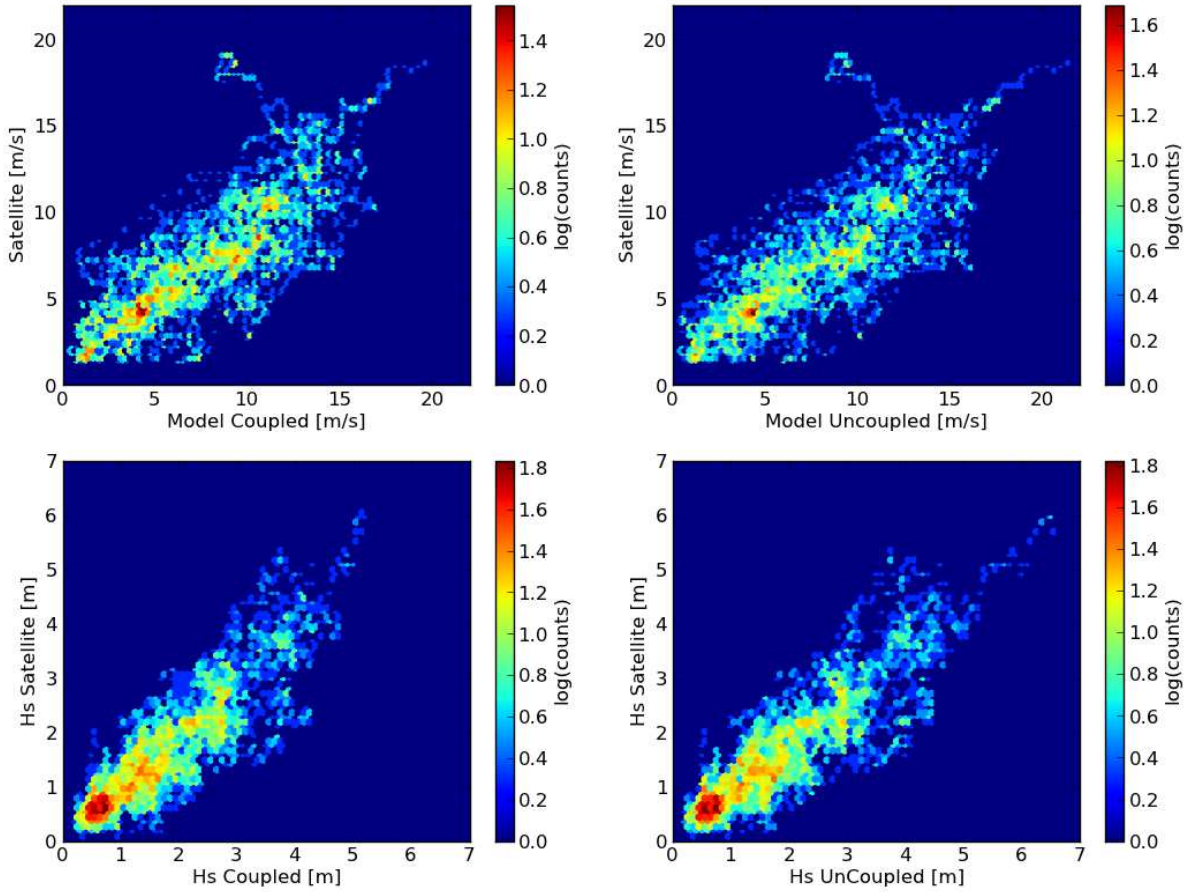

Figure VI.8: Comparison of winds and waves for ERS-2.

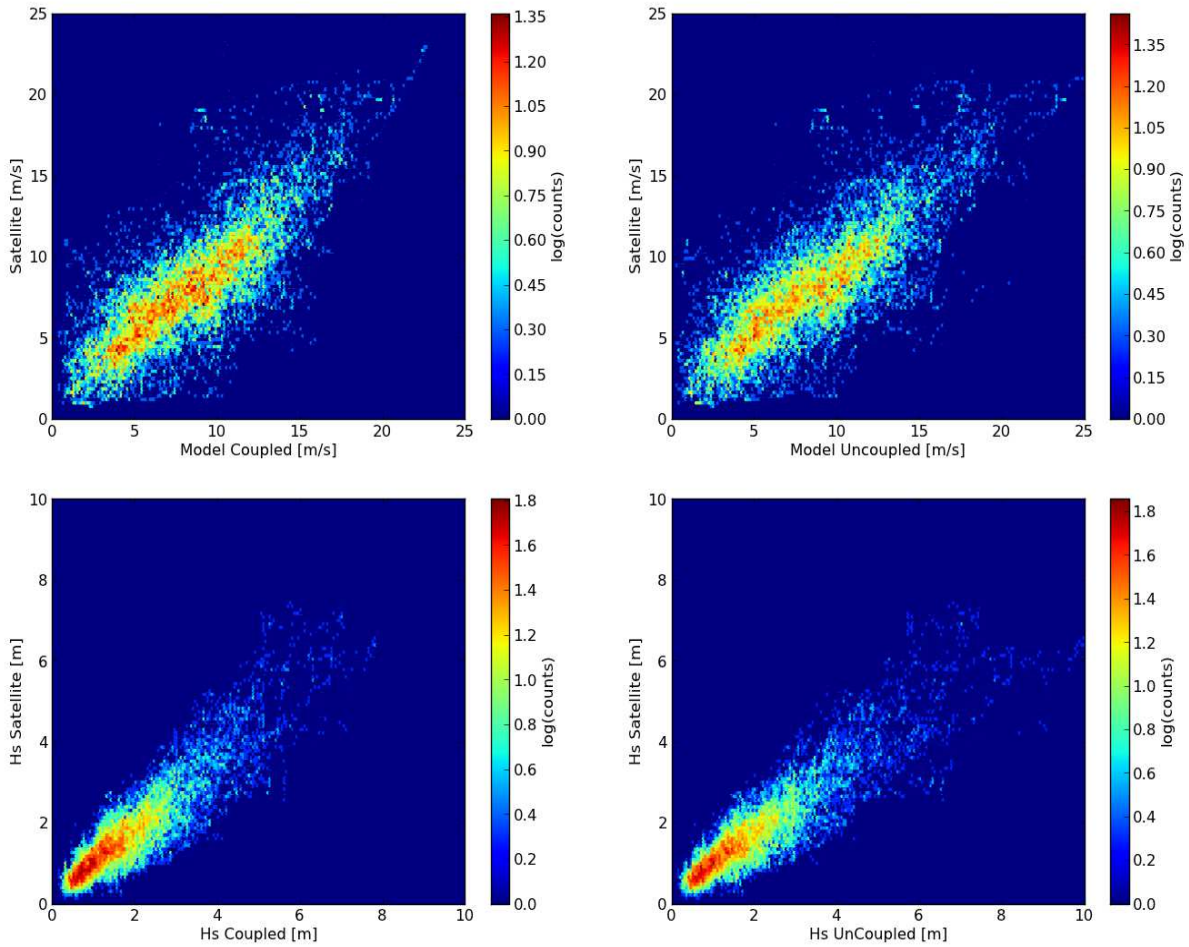

Figure VI.9: Comparison for all Altimeters (ERS-2, Envisat, Jason-1, Jason-2.)

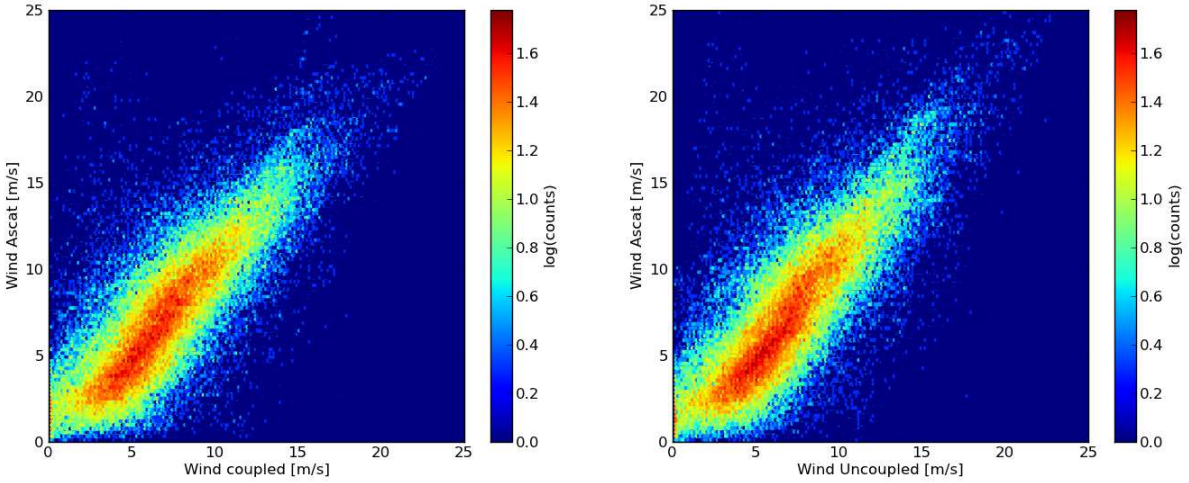

Figure VI.10: Comparison of the waves for ASCAT.

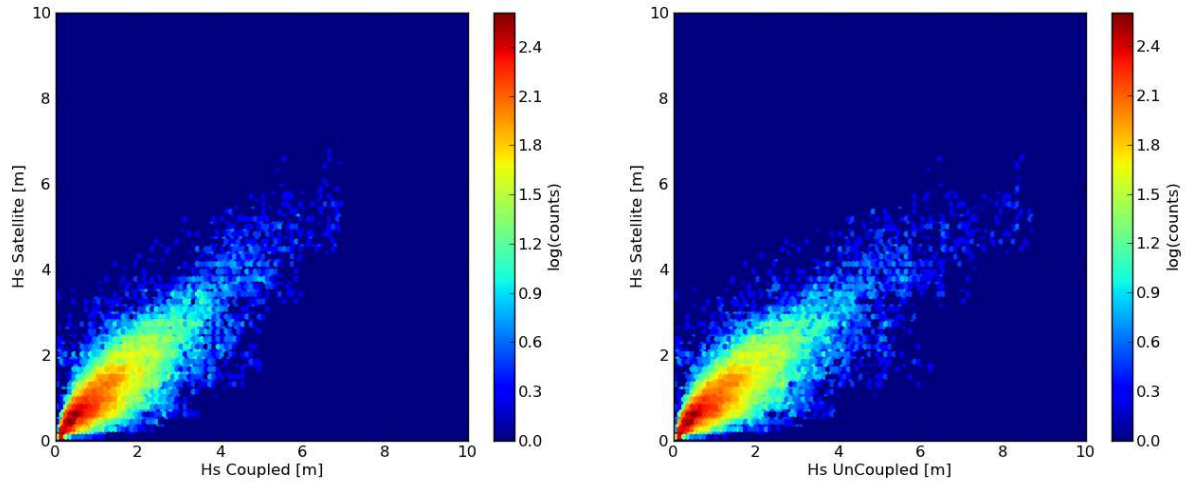

Figure VI.11: Ccomparison of the waves for all 36 in-situ buoys of the Mediterranean.

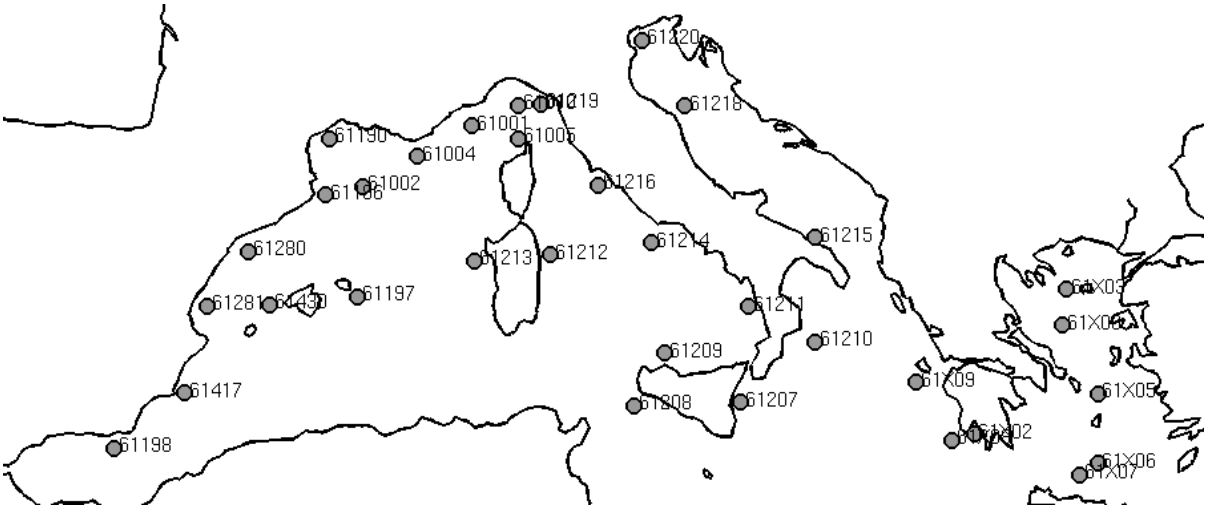

Figure VI.12: Comparison of the waves for all 36 in-situ buoys of the Mediterranean.

Figure VI.12Table VI-1: Statistics based on ERS-2 data

		ME	AE	RMSE	CRMSE	Corr	sci	sciR
Waves	Coup	0.11	0.37	0.5	0.49	0.88	0.31	0.3
	Uncoup	0.24	0.43	0.58	0.53	0.88	0.36	0.32

		ME	AE	RMSE	CRMSE	Corr	sci	sciR
Wind	Coup	0.49	1.8	2.48	2.43	0.79	0.35	0.34
	Uncoup	0.63	1.89	2.59	2.52	0.79	0.36	0.35

	Wave			Wind			
Period	ME	AE	RMSE	ME	AE	RMSE	
11/11/2010	-0.21	0.34	0.43	0.26	1.34	1.78	NbPt=856
11/21/2010	0.14	0.23	0.31	0.44	1.44	1.89	NbPt=876
12/1/2010	-0.01	0.29	0.4	-0.77	2.05	3.18	NbPt=824
12/11/2010	0.25	0.38	0.56	0.81	1.63	2.24	NbPt=1200
12/21/2010	0.18	0.55	0.66	1.39	2.78	3.37	NbPt=838
12/31/2010	0.26	0.41	0.54	0.66	1.66	2.16	NbPt=908

	Wave			Wind		
Period	ME	AE	RMSE	ME	AE	RMSE
11/11/2010	-0.1	0.37	0.47	0.43	1.44	1.88
11/21/2010	0.21	0.28	0.38	0.43	1.46	1.93
12/1/2010	0.1	0.33	0.44	-0.68	2.15	3.25
12/11/2010	0.36	0.46	0.67	1.07	1.85	2.54
12/21/2010	0.37	0.61	0.73	1.51	2.72	3.31
12/31/2010	0.4	0.49	0.65	0.79	1.82	2.37

Table VI-2: Statistics based on ENVISAT data

		ME	AE	RMSE	CRMSE	Corr	sci	sciR
Waves	Coup	0.25	0.46	0.65	0.6	0.88	0.34	0.32
	Uncoup	0.43	0.57	0.85	0.73	0.88	0.45	0.39

		ME	AE	RMSE	CRMSE	Corr	sci	sciR
Wind	Coup	0.25	1.71	2.28	2.26	0.81	0.26	0.25
	Uncoup	0.44	1.87	2.44	2.4	0.81	0.27	0.27

	Wave			Wind			
Period	ME	AE	RMSE	ME	AE	RMSE	
11/11/2010	-0.11	0.26	0.35	-0.39	1.14	1.59	NbPt=820
11/21/2010	0.14	0.28	0.38	0.12	1.51	2.04	NbPt=636
12/1/2010	0.13	0.33	0.46	0.11	1.88	2.5	NbPt=927
12/11/2010	0.19	0.46	0.63	0.14	1.58	2.05	NbPt=995
12/21/2010	0.62	0.82	1.02	0.83	2.01	2.69	NbPt=1220
12/31/2010	0.33	0.41	0.54	0.42	1.94	2.36	NbPt=945

	Wave			Wind		
Period	ME	AE	RMSE	ME	AE	RMSE
11/11/2010	0.02	0.25	0.39	-0.25	1.22	1.61
11/21/2010	0.25	0.37	0.52	0.3	1.68	2.34
12/1/2010	0.23	0.38	0.54	0.27	1.97	2.64
12/11/2010	0.36	0.52	0.77	0.38	1.57	2.05
12/21/2010	0.98	1.09	1.36	1.25	2.43	3.04
12/31/2010	0.45	0.53	0.77	0.32	2.06	2.43

Table VI-3: Statistics based on Jason-1 data.

		ME	AE	RMSE	CRMSE	Corr	sci	sciR
Waves	Coup	0.13	0.39	0.54	0.52	0.90	0.31	0.30
	Uncoup	0.29	0.47	0.71	0.65	0.90	0.42	0.38

		ME	AE	RMSE	CRMSE	Corr	sci	sciR
Wind	Coup	0.09	1.59	2.12	2.12	0.81	0.25	0.25
	Uncoup	0.23	1.71	2.25	2.24	0.82	0.27	0.26

	Wave			Wind			
Period	ME	AE	RMSE	ME	AE	RMSE	
11/11/2010	-0.16	0.27	0.31	-0.33	1.03	1.30	NbPt=1119
11/21/2010	-0.01	0.20	0.27	-0.29	1.43	1.86	NbPt=1291
12/1/2010	0.04	0.28	0.37	0.19	1.33	1.72	NbPt=1402
12/11/2010	0.03	0.31	0.42	-0.07	1.23	1.70	NbPt=1453
12/21/2010	0.24	0.53	0.67	-0.39	2.27	2.95	NbPt=1480
12/31/2010	0.65	0.74	0.89	1.53	2.18	2.61	NbPt=1248

	Wave			Wind		
Period	ME	AE	RMSE	ME	AE	RMSE
11/11/2010	-0.01	0.26	0.33	-0.08	1.03	1.32
11/21/2010	0.07	0.23	0.34	-0.24	1.36	1.77
12/1/2010	0.10	0.28	0.38	0.24	1.35	1.73
12/11/2010	0.16	0.37	0.55	0.02	1.43	1.91
12/21/2010	0.51	0.70	0.90	-0.25	2.49	3.13
12/31/2010	0.90	0.97	1.26	1.77	2.47	2.89

Table VI-4: Statistics based on Jason-2 data.

		ME	AE	RMSE	CRMSE	Corr	sci	sciR
Waves	Coup	0.11	0.37	0.5	0.49	0.88	0.31	0.3
	Uncoup	0.24	0.43	0.58	0.53	0.88	0.36	0.32

		ME	AE	RMSE	CRMSE	Corr	sci	sciR
Wind	Coup	0.17	1.57	2.08	2.08	0.82	0.27	0.27
	Uncoup	0.32	1.63	2.13	2.11	0.82	0.28	0.27

	Wave			Wind			
Period	ME	AE	RMSE	ME	AE	RMSE	
11/11/2010	-0.24	0.29	0.39	-0.35	1.18	1.52	NbPt=1449
11/21/2010	-0.05	0.22	0.28	0.14	1.3	1.67	NbPt=1268
12/1/2010	0.14	0.31	0.4	0.08	1.47	1.86	NbPt=1689
12/11/2010	0.08	0.28	0.39	0.28	1.33	1.73	NbPt=1500
12/21/2010	0.24	0.41	0.52	-0.18	2.22	2.84	NbPt=1668
12/31/2010	0.33	0.45	0.61	1.04	1.79	2.41	NbPt=1540

	Wave			Wind		
Period	ME	AE	RMSE	ME	AE	RMSE
11/11/2010	-0.14	0.28	0.37	-0.26	1.24	1.58
11/21/2010	0.01	0.22	0.28	0.18	1.33	1.71
12/1/2010	0.25	0.37	0.49	0.21	1.51	1.93
12/11/2010	0.13	0.31	0.42	0.3	1.42	1.83
12/21/2010	0.41	0.51	0.66	0.26	2.19	2.72
12/31/2010	0.47	0.52	0.74	1.19	1.99	2.62

Table VI-5: Statistics based on In-Situ buoys.

	ME	AE	RMSE	CRMSE	Corr	sci	sciR
Coup	0.11	0.39	0.55	0.54	0.77	0.42	0.42
Uncoup	0.21	0.43	0.62	0.58	0.77	0.48	0.45

Table VI-6: Wind Statistics based on ASCAT data

Coup	ME=0.61	AE=1.93	RMSE=2.56
Uncoup	ME=0.77	AE=2.04	RMSE=2.69

VI.2 System implementation and verification (MS2, period M0+18:M0+30) (HCMR)

The system has been tested and evaluated in a number of preselected case studies related to the development of extreme sea state conditions in the Mediterranean Sea. In this framework WEW is compared to the offline coupled simulations (CTRL), in which the Charnock parameter is kept constant throughout the atmospheric simulation and the ocean-wave model retrieves wind field updates on hourly basis (3600 sec).

VI.2.1 Interactions and system sensitivity

In the CTRL and WEW experiments, the Charnock coefficient increases logarithmically with the wind speed at about the 22 ms^{-1} (Figure VI.13). Especially in WEW, the saturation of Charnock coefficient for wind speeds exceeding the 22 ms^{-1} indicates that in cyclonic wind conditions the sea surface friction conserves or decreases offering a positive forcing to the flow. This finding has been also confirmed by relevant studies (eg. Makin 2005).

The enhanced Charnock coefficient increases the roughness length and results in a decrease of the near surface wind speed in WEW simulations. This in turn affects the wind input turn and finally the estimation of the significant wave height in the two-way coupled simulations.

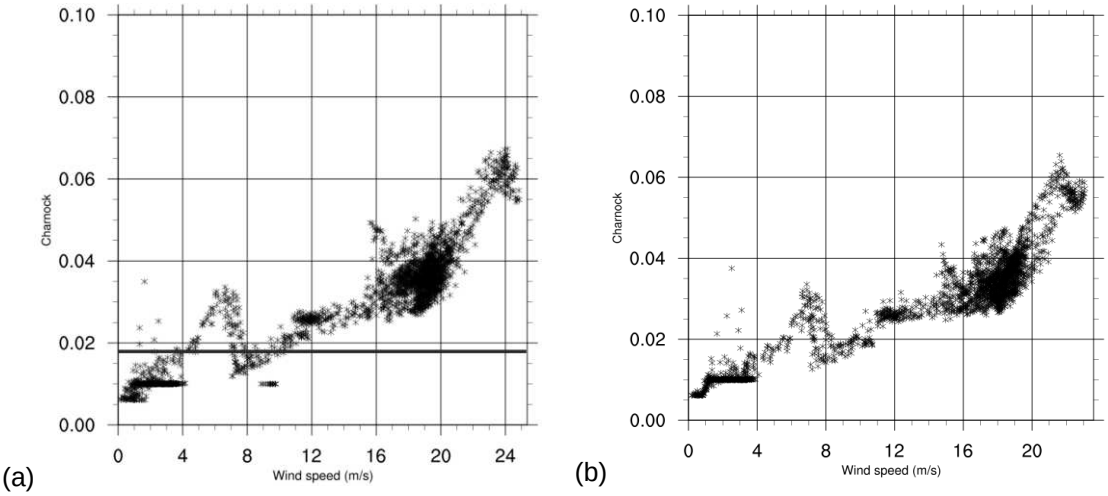

Figure VI.13: Charnock coefficient dependence on the wind speed in (a) offline coupled simulations. The thick solid line indicates the constant Charnock value of 0.018. (b) WEW simulations.

The roughness length as a function of the friction velocity is shown in Figure VI.14 for the CTRL (a) and WEW (b) runs. The roughness length increases exponentially with the friction velocity in moderate and rough sea state regimes. In WEW experiment, the roughness length is substantially larger than in CTRL for friction velocities exceeding the 0.40 ms^{-1}. This is an indication of the enhanced friction in WEW under rough sea state regimes as a result of the usage of a variable Charnock parameter in the surface layer parameterization scheme.

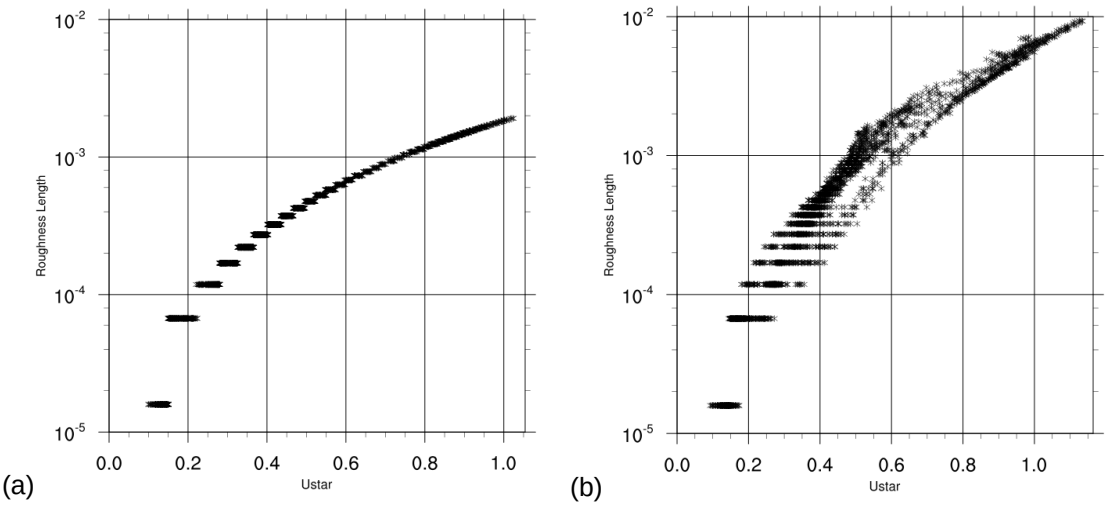

Figure VI.14: Roughness length (m) dependence to the friction velocity (ms-1) for (a) the CTRL and (b) WEW experiments.

VI.2.2 Case studies and methodology

After the first phase of the coupled system development, WEW was tested for its consistency and performance in high-impact atmospheric and sea state case studies. The performance of the fully two-way coupled system (WEW) was statistically evaluated over sea and land areas against its performance in the offline coupling mode (CTRL). The evaluation was based on the point-to-point comparison with remote sensed and in situ observations for four preselected cases/events of atmospheric and sea state development significance. These cases are the following:

A) **4-11 January 2012**;

B) **21-28 March 2011**;

C) **9-13 December 2010**;

D) **3-6 May 2010**.

Analytical description of the atmospheric conditions prevailed in the cases A-D is presented in section VI.2.2. The WEW performance for the abovementioned cases has been assessed using as reference the network of 39 available buoys in the Mediterranean Sea (Figure VI.12).

The system is also evaluated against remote sensed data retrieved from CRYOSAT, ENVISAT, ESR2 and JASON1/2 (Figure VI.15). The sensitivity of the system is also assessed over land at the positions of almost 500 surface meteorological stations across Europe, Middle East and Northern Africa (Figure VI.16).

The data processing and the statistical evaluation are based on the NCAR Command Language (NCL, 2014). The software developed (based on NCL) includes modules for the post-processing of the system outputs in GRIB-1 format and a new statistical package. In the decoding procedure, the GRIB-1 data is initially converted to the intermediate ascii data which is then applied for the estimation of the statistical indexes valid for both continuous and discrete variables. The use of intermediate ascii files supports a quick and safe approach for the evaluation and allowed a simple debugging at the same time. The software has been developed in a modular and effective way; it is flexible and allows an easy configuration under various environments and platforms. The scores are finally redirected in text outputs and visualized in the form of spatial maps, X-Y plots, scatter plots, box plots and Taylor diagrams (Taylor, 2005).

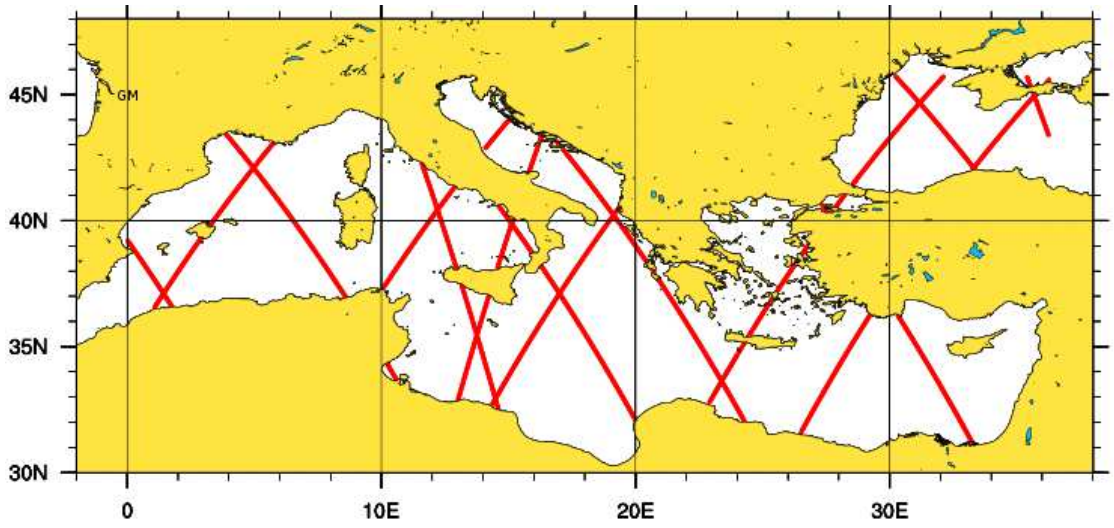

Figure VI.15: Indicative satellite retrievals used for the evaluation of the system. Data source: Globwave project (http://globwave.ifremer.fr).

The evaluation methodology is based on the point-to-point hourly comparison between model-generated variables and the observations (Wilks, 1995). The gridded outputs are interpolated to each buoy location using the nearest-neighbor interpolation scheme. Consequently, thousands pairs of model outputs and observations produced for both the offline coupled (CTRL) and the fully coupled (WEW) system modes. The verification procedure is based on the estimation of traditional objective verification techniques such as the standard mean error (Bias), and the root mean square error (RMSE) for continuous predictands (wind speed and the significant wave height). Also, mean value (Mean), standard deviation (STD) and Scatter Index (SI) are also calculated for both model and observed values. Supplementary scores are also the Pearson correlation coefficient and the coefficient of determination (R^2). Please refer to Annex A for metrics definitions.

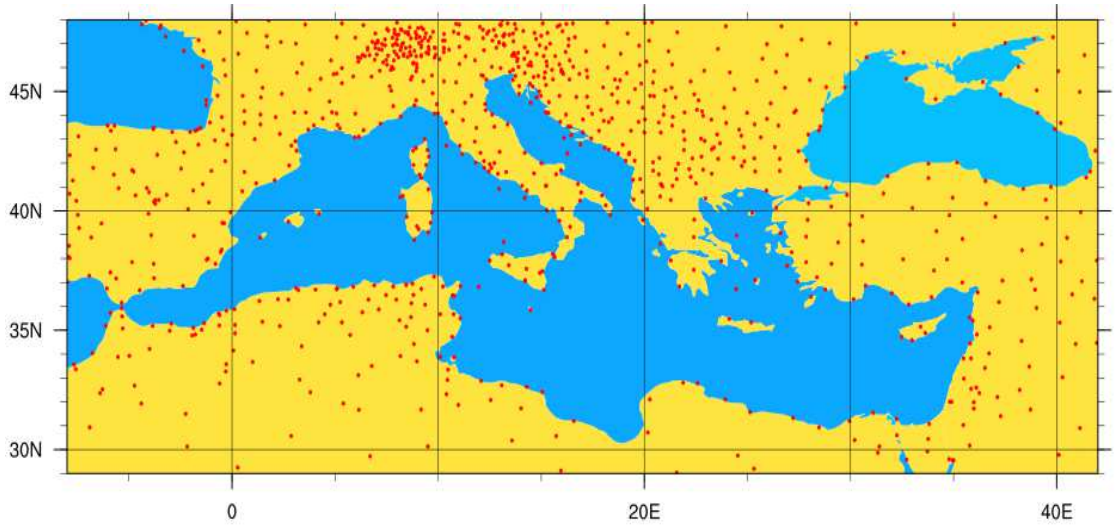

Figure VI.16: Spatial distribution of the land surface stations applied for the evaluation of the system. Data source: ECMWF-GTS network.

The software also includes an advanced quality control package in order to remove the erroneous measurements, based on checking the physical range of each parameter being verified, the allowable rate of change in time and the stationarity. Furthermore, to avoid accuracy issues of the buoys and the remote sensed sensors, wind speed values lower than 1 ms^{-1} and significant wave height values lower than 0.2 m were excluded from the statistical evaluation.

An overall evaluation of the system was also performed over land against a number of land surface observations obtained from the GTS network (Figure VI.16). The extracted scores are the standard

mean error (Bias) and the root mean square error (RMSE) for the basic continuous predictands (wind speed, temperature and mean sea level pressure). The verification scores used for the discrete variable (precipitation) are based on the contingency table approach (Wilks, 1995). This is a two-dimensional matrix where each element counts the number of occurrences in which the gauge measurements and the model forecasts exceeded or failed to reach a certain threshold for a given forecast period (Papadopoulos and Katsafados 2009). The table elements are defined as: A- model forecast and gauge measurement exceeded the threshold; B- model forecast exceeded the threshold but measurement not; C- model forecast did not reach the threshold but measurement exceeded it; and D- model forecast and measurement did not reach the threshold. Considering the above elements the forecast skill can be measured by evaluating the bias score (BS) and the equitable threat score (ETS). Thus, the bias score is defined as

$$BS = \frac{A+B}{A+C} \tag{27}$$

while the ET score defined as

$$ETS = \frac{A-E}{A+B+C-E} \tag{28}$$

and E is defined by

$$E = \frac{F \times O}{N} = \frac{(A+B)\times(A+C)}{N} \tag{29}$$

with N holding the total number of observations being verified (N=A+B+C+D). The introduction of the E term (Mesinger, 1996) is an enhancement to the normal threat score (as defined in Wilks, 1995); since it reduces it by excluding the number of randomly forecast “hits”. Computing the bias and the equitable threat scores, a measurement of the model accuracy on the frequency of occurrences at or above a certain precipitation threshold amount can be revealed (Papadopoulos et al., 2005). Consequentially, at given thresholds the bias score can represent a systematic overestimation (when BS > 1) or underestimation (when BS < 1), and the ET score can present poor forecasts (when ETS ≈ 0) or perfect forecasts (when ETS=1). To measure the magnitude of the difference between model forecast and observed precipitation the root mean square error (RMSE) was also calculated as follows (Colle et al., 2000; Mass et al., 2002):

$$RMSE = \sqrt{\frac{\sum_{i=1}^{N}(MP_i - OP_i)^2}{N}} \tag{30}$$

where MP_i and OP_i are the model-estimated and the observed precipitation, respectively, and the N is the total number of observations at a specific location reaching or exceeding a certain threshold amount. Combining these statistical criteria we attempt to provide a comprehensive evaluation of system performance. For example, a greater ETS will represent a significant model improvement only if it is accompanied by a BS with value close to one and a lowering RMSE. Another widely used score for verifying precipitation is the Heidke skill score (HSS; Heidke 1926). It is estimated based on the contingency table elements from the expression:

$$HSS = \frac{2(A\times D - B\times C)}{(A+C)\times(C+D)\times(A+B)\times(B+D)} \tag{31}$$

VI.2.3 Synoptic analysis of the case studies A-D

VI.2.3.1Case A)

The incident of **4–11 January, 2012,** has been selected due to the severity of the prevailed atmospheric conditions characterized by an explosive cyclogenesis in Ligurian Sea (Varlas et al., 2014). In more details, on January 5, 2012 a low pressure system was formed over the cyclogenetic area of the Ligurian Sea. On January 6 the system was moved towards the Eastern Mediterranean,

where the pressure dropped more than 24sinφ/sin60˚ hPa in 24 h, defining the event as explosive cyclogenesis event. During January 6 and 7, the strong pressure gradient provoked gale force winds and significant storm surge over a vast area including Central Mediterranean and the Aegean Sea. It is noteworthy that the buoys at the Ligurian and Balearic Seas recorded wind speeds exceeding 20 ms^{-1} and significant wave height over 5m.

VI.2.3.2Case B)

On **March 21-24, 2011,** a series of barometric lows affected Greece and provoked northeastern gale force winds over the Aegean Sea. Moreover, on March 23 at 00 UTC a barometric low with fronts organized over Western Algeria and resulted in eastern-northeastern gale force winds over the Gibraltar Straits.

VI.2.3.3Case C)

On **December 9, 2010,** a well-organized barometric low system with accompanied fronts passed over Italy and Greece. The system was supported from a rapidly extended trough from the central and northern Europe and provoked northeastern gale force winds over Aegean Sea. The system was further deepened on December 11 due to the meridional trough existence over northeastern Europe caused more intense winds especially over southeastern Mediterranean Sea.

VI.2.3.4Case D)

On **May 3, 2010**, a barometric low was formed over the cyclogenetic area of Balearic Islands. The surface convergence was combined with a divergent zone in front of an easterly propagated trough which supported the system with upper air cold advection. Next day the surface system was further deepened and provoked gale force winds at the Gulf of Lions.

VI.2.4 Statistical analysis of the case study A (January 4-11, 2012)

The outputs from both simulations, offline coupled (CTRL) and fully coupled (WEW), have been statistically evaluated based on the point-to-point hourly comparison between model-generated variables and the available Mediterranean buoys measurements. For the case study (A), both simulations seem to slightly overestimate the near surface wind speed exceeding 1 ms^{-1}. The overestimation is more pronounced for wind speeds up to 8 ms^{-1} (Figure VI.17). WEW represents an overall improvement of the RMS error by approximately 0.5%. Also, WEW decreases the standard deviation (STD Mod) and preserves R^2 and SI indexes. Nevertheless, CTRL shows a slightly better correlation (Pearson index) and mean value closer to mean value of observations. The bias scores of the significant wave height (SWH) indicate a systematic overestimation for the CTRL simulation which turns into slight underestimation in WEW (Figure VI.18). WEW also offers an overall improvement up to 3.6% of the SWH error and increased correlation coefficients.

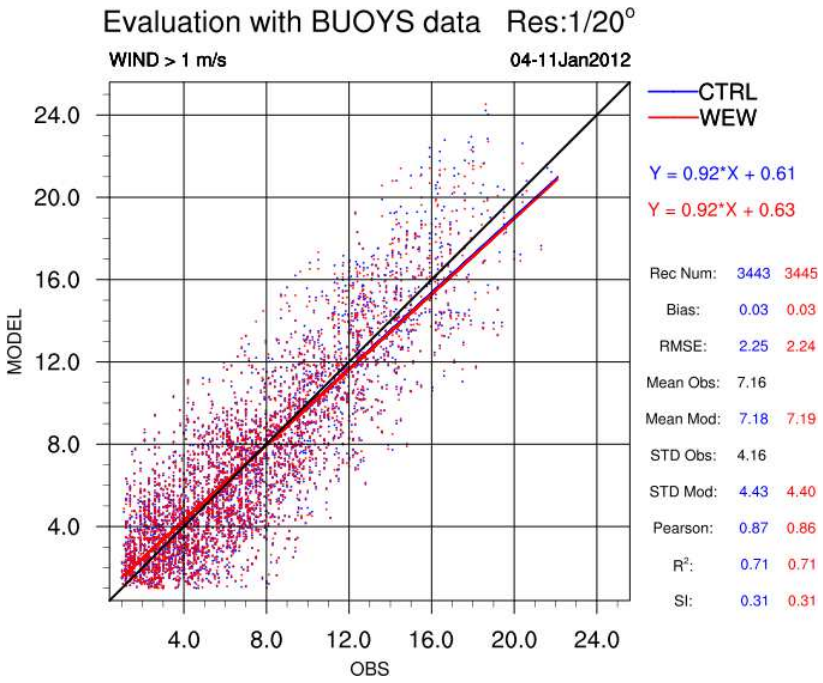

Figure VI.17: Scatter plot for near surface wind speed exceeding 1 ms^{-1}. Y-axis represents the model-estimated values and X-axis the buoys observations. CTRL and WEW evaluation results are shown in blue and red colors respectively.

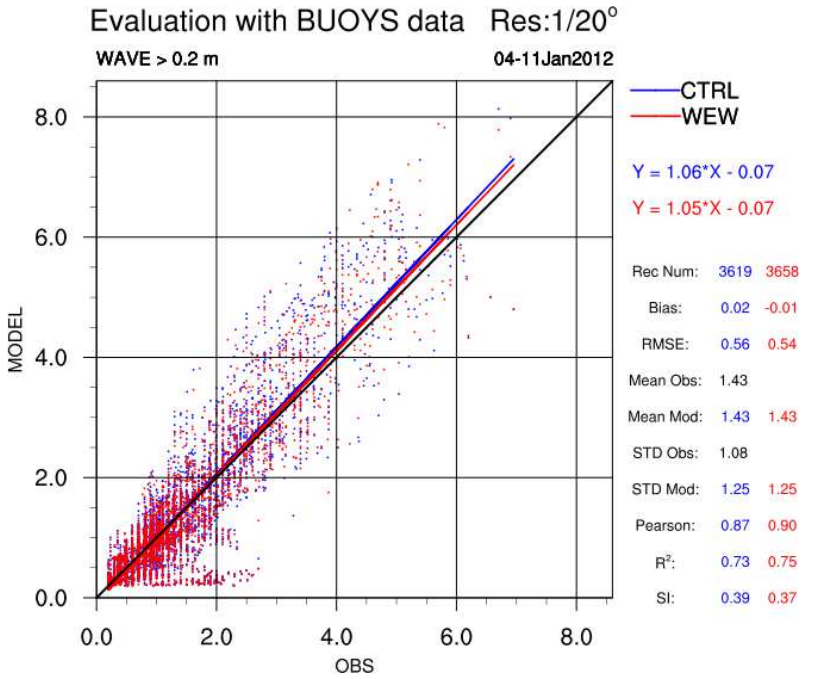

Figure VI.18: As in Figure VI.17 for the significant wave height exceeding 0.2m.

The system has been also evaluated against remote sensed data. In contrast to the overestimation with the buoys comparison, a systematic underestimation of the wind speed is evidenced for both CTRL and WEW simulations. WEW also reduces the RMSE up to 2.5% (Figure VI.19). Furthermore, a decrease of the STD, an improvement of R^2 up to 2.7% and a conservation of the rest indexes values are also evidenced. The comparison against satellite retrievals indicated that both CTRL and WEW simulations systematically overestimate the SWH (Figure VI.20). WEW further improves the entire statistical scores and shows a RMSE decrease by almost 7%. The above indexes are also statistically significant in 95% confidence level.

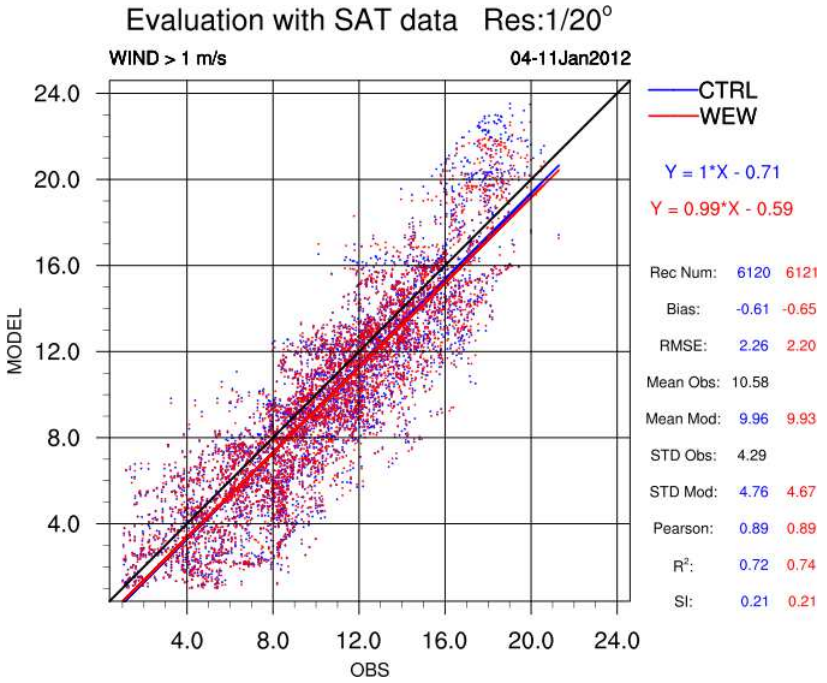

Figure VI.19: As in Figure VI.17 for the near surface wind speed exceeding 1 ms^{-1}.

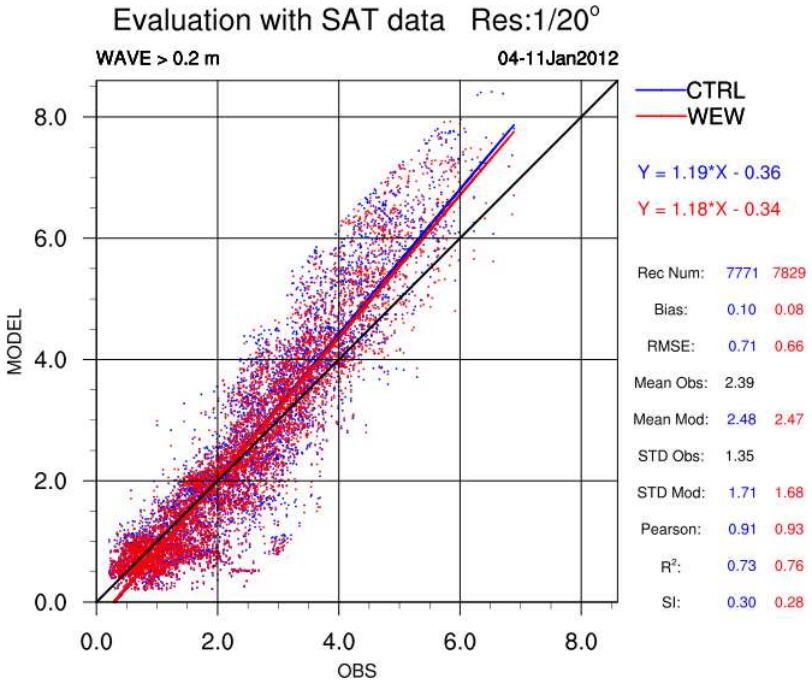

Figure VI.20: As in Figure VI.17 for the significant wave height exceeding 0.2m.

VI.2.5 Statistical analysis of the case study B (March 21-28, 2011)

The statistical scores for both wind speed and SWH are almost identical for CTRL and WEW runs (Figure VI.21, Figure VI.22). The systematic overestimation for the wind speed turns to underestimation for the SWH. Lower and moderate velocities mostly contribute to the overestimation. WEW slightly improves the wind speed R^2 index and it marginally decreases the SWH STD up to 1.8%.

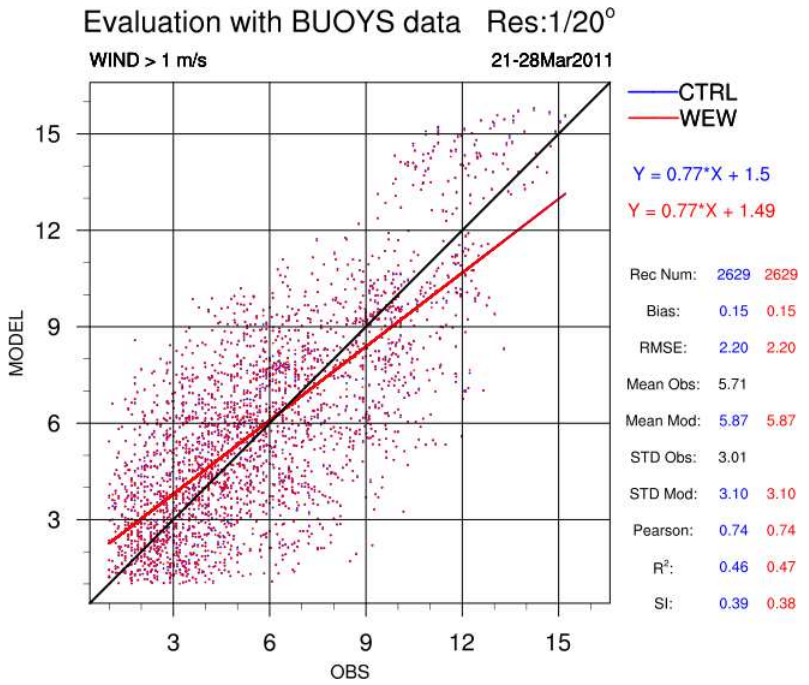

Figure VI.21: Scatter plot for near surface wind speed exceeding 1 ms^{-1}. Y-axis represents the model-estimated values and X-axis the buoys observations. CTRL and WEW evaluation results are shown in blue and red colors respectively.

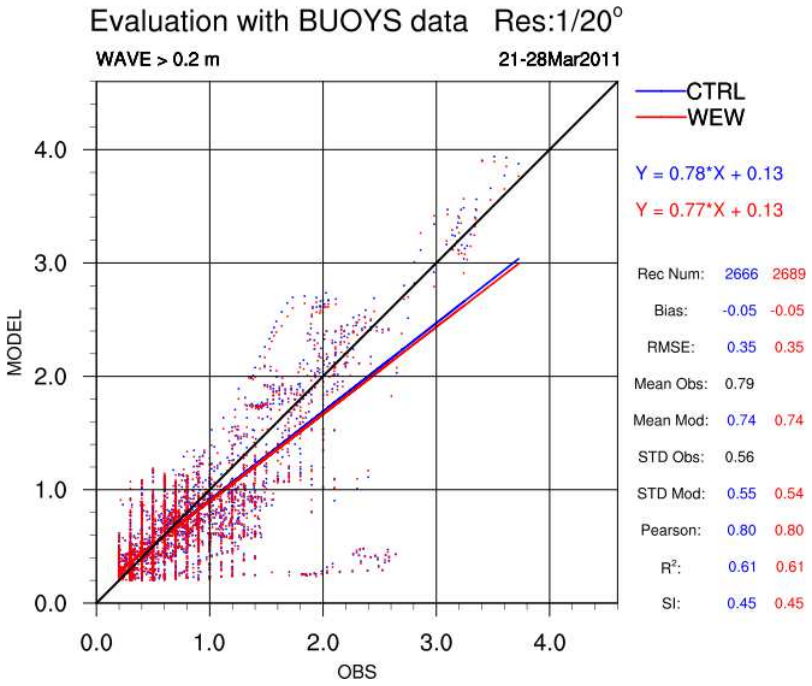

Figure VI.22: As in Figure VI.21 for the significant wave height exceeding 0.2m.

Against satellite retrievals, both simulations overestimate the wind speed but WEW provides slight Bias, STD and mean value improvements (Figure VI.23). The overestimation is more prominent for the wind speeds lower than 7 ms^{-1}. The SWH is systematically underestimated by both runs (Figure VI.24). WEW slightly increases the underestimation for the heights exceeding the 1m.

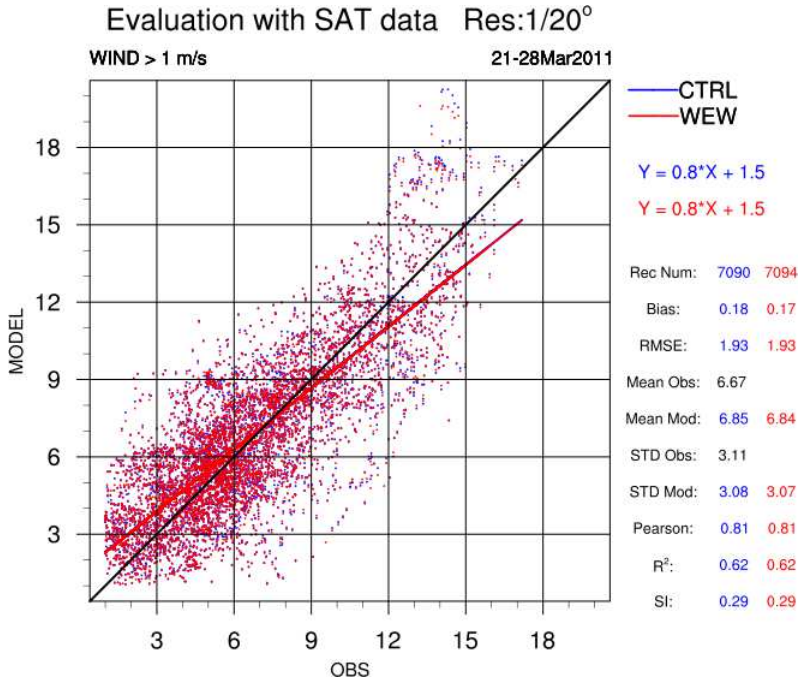

Figure VI.23: As in Figure VI.21 for the near surface wind speed exceeding 1 ms^{-1}.

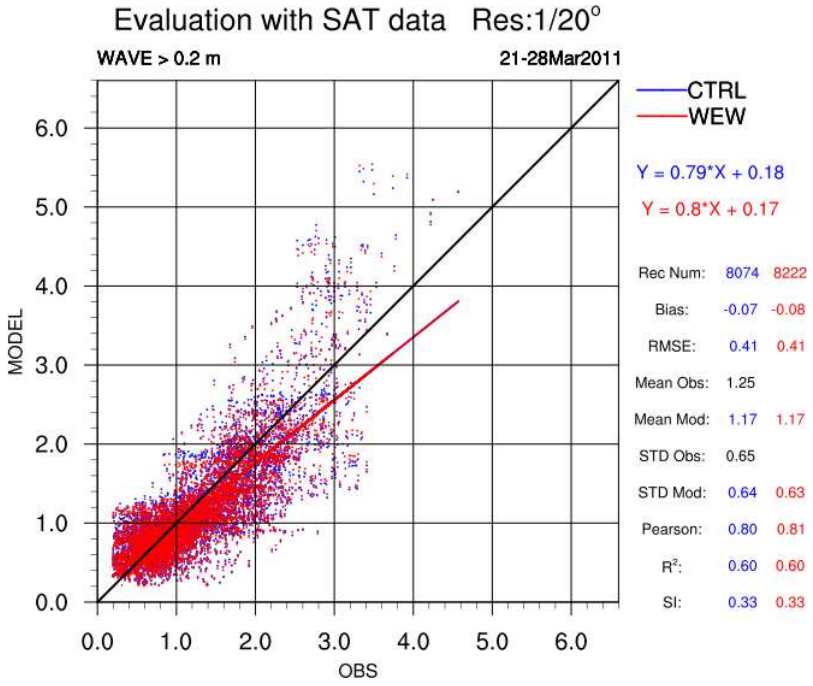

Figure VI.24: As in Figure VI.21 for the significant wave height exceeding 0.2m.

VI.2.6 Statistical analysis of the case study C (December 9-13, 2010)

A substantial response of the statistical indexes is evidenced in this case study. Despite the fact that both runs overestimate the wind speed, the WEW decreases the Bias error and improves up to 2.4% the RMSE and the STD (Figure VI.25). There are also improvements in Mean value, in SI (up to 3.7%) and in R^2 (up to 2.8%). The overall improvement in the wind speed is marginally reflected to the SWH indexes. In more details, WEW shows reduced RMSE by 1.7%, STD by 2.2%, R^2 by 6.8% and scatter index up to 1.7% (Figure VI.26).

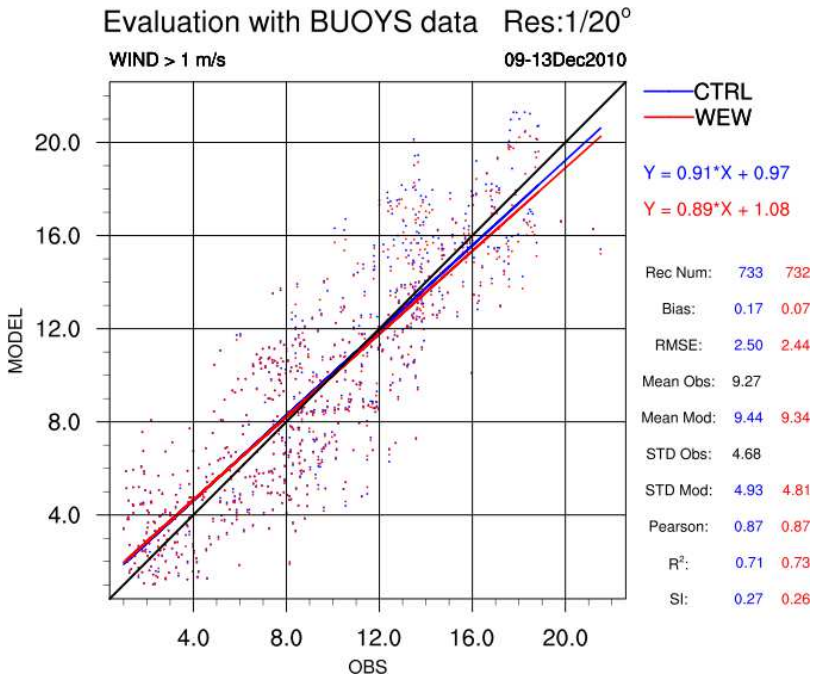

Figure VI.25: Scatter plot for near surface wind speed exceeding 1 ms^{-1}. Y-axis represents the model-estimated values and X-axis the buoys observations. CTRL and WEW evaluation results are shown in blue and red colors respectively.

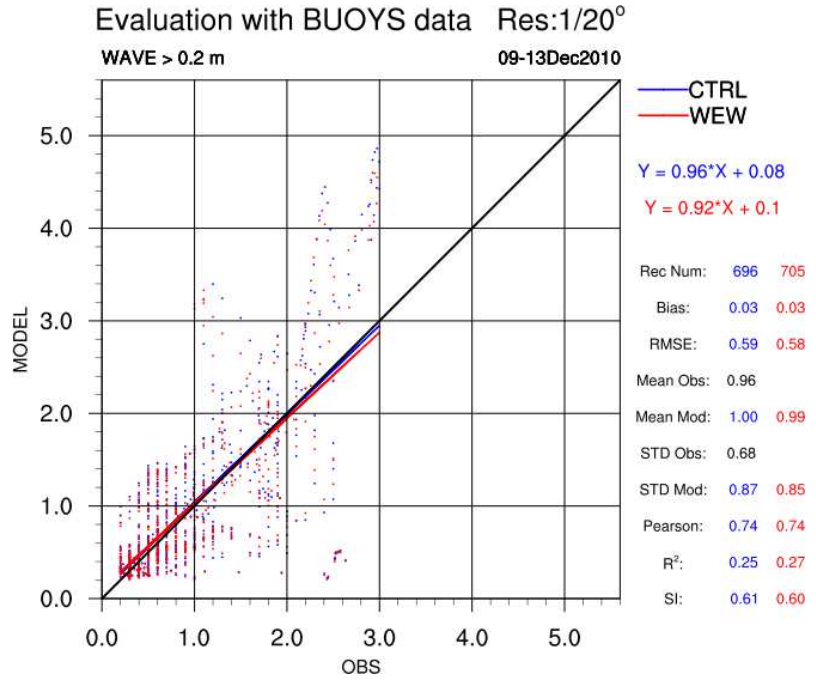

Figure VI.26: As in Figure VI.25 for the significant wave height exceeding 0.2m.

Both CTRL and WEW underestimate the wind speed more prominent for velocities exceeding the 8 ms^{-1} (Figure VI.27). Despite the fact of the increased underestimation, WEW presents an overall RMSE improvement up to 1.7%, better R^2 per 1.4% and finer STD per 2.6%. In contrast to the wind speed, both simulations overestimate the SWH more prominent for the heights exceeding the 1m (Figure VI.28). However, WEW is substantially decreases the overestimation with an overall bias of 0.01 instead of the 0.04. It is also improves the RMS error by 3.2% and it shows an overall better fit with the remote sensed data.

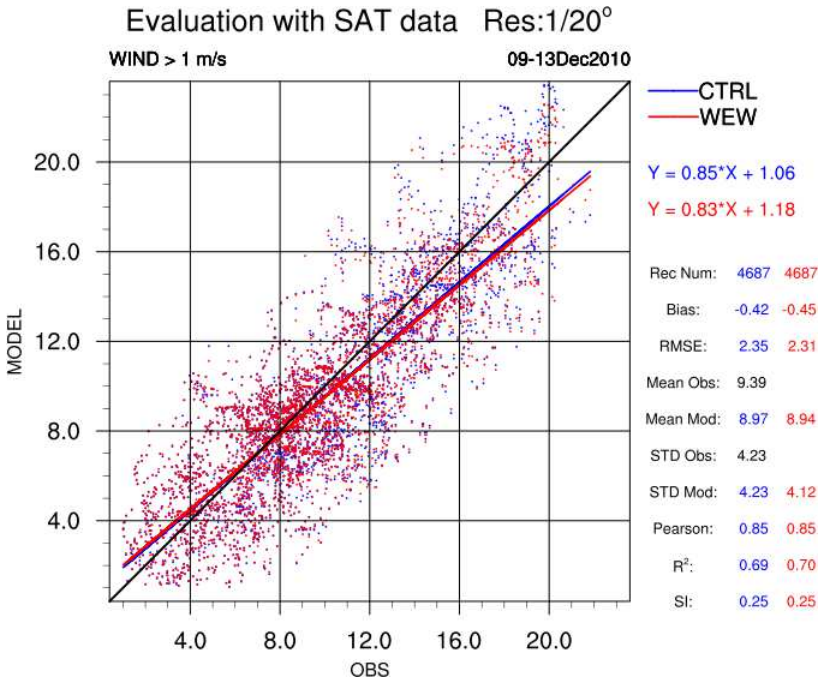

Figure VI.27: As in Figure VI.25 for the near surface wind speed exceeding 1 ms^{-1}.

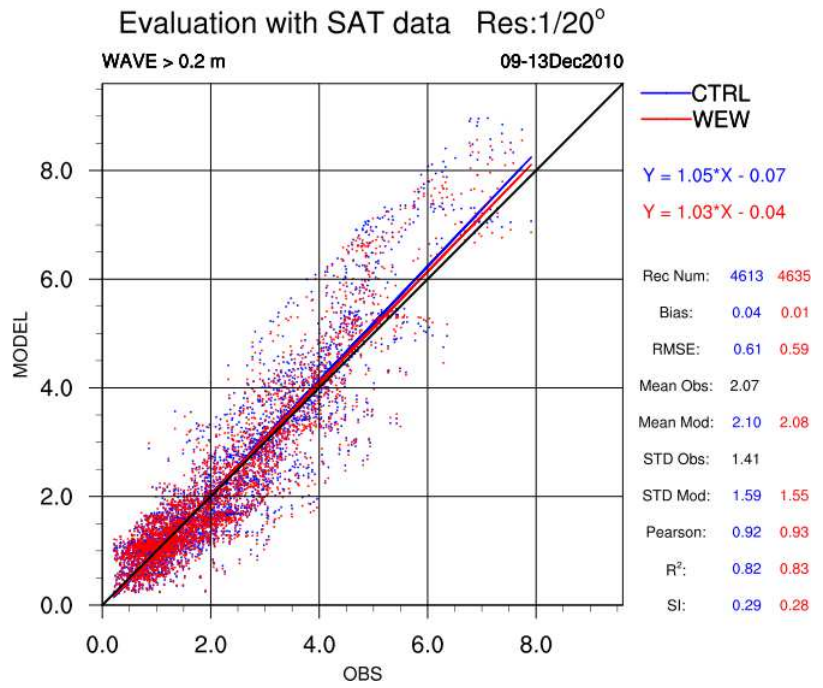

Figure VI.28: As in Figure VI.25 for the significant wave height exceeding 0.2m.

VI.2.7 Statistical analysis of the case study D (May 3-6, 2010)

This final case is characterized from limited number of the available buoys observations. Both runs significantly overestimate the wind speed and especially the light to moderate winds (Figure VI.29). SWH is underestimated by both models more prominent for the CTRL (Figure VI.30). WEW reduces the RMSE by 2% and offers an overall improvement for the rest indexes by 1-2%. The above scores do not consider as statistically significant due to the small sample of data.

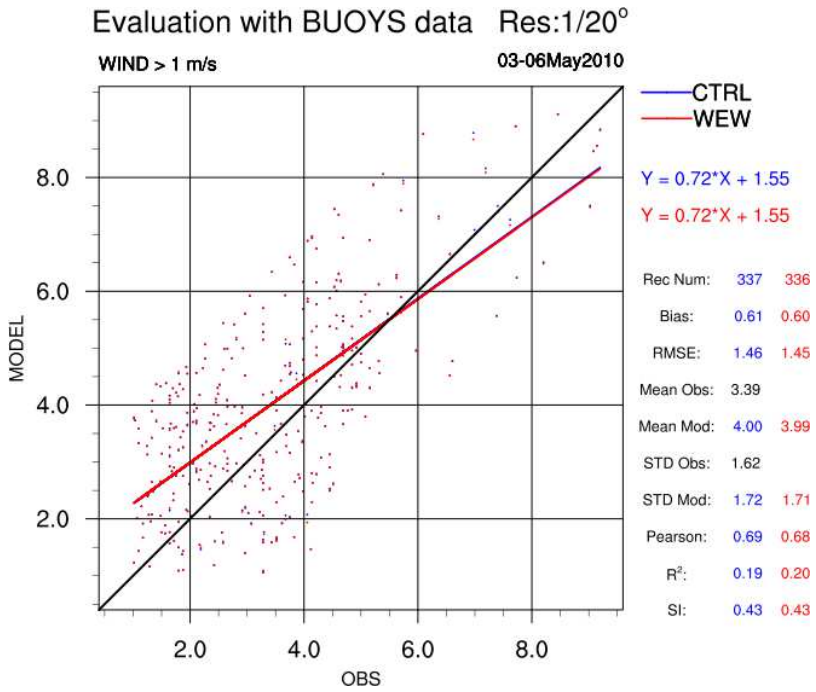

Figure VI.29: Scatter plot for near surface wind speed exceeding 1 ms^{-1}. Y-axis represents the model-estimated values and X-axis the buoys observations. CTRL and WEW evaluation results are shown in blue and red colors respectively.

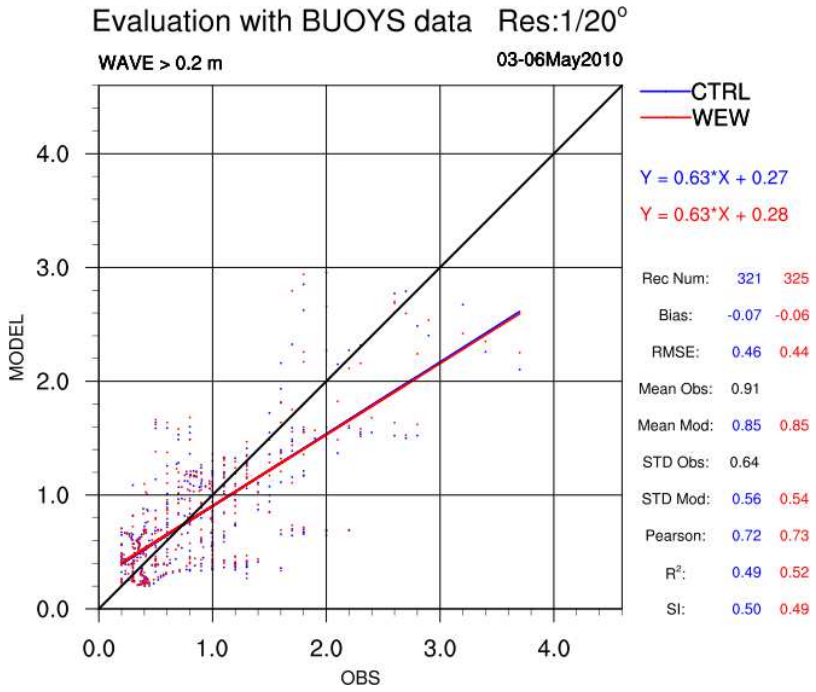

Figure VI.30: As in Figure VI.29 for the significant wave height exceeding 0.2m.

The comparison against remote sensed data reveals substantial improved scores and a significantly increased sample of data. WEW shows a marginal improvement of the Bias and RMS errors. Both runs overestimate the wind speeds up to 7 ms^{-1} and underestimate above (Figure VI.31). Similar to the wind speed, an overestimation is observed for the SWH up to 1.5 m which turns to underestimation for higher values (Figure VI.32). WEW offers a consistent improvement of the Bias and the RMS errors up to 4% and an overall correlation increase by 3%. The entire indexes have been tested as statistically significant in the 95% confidence level.

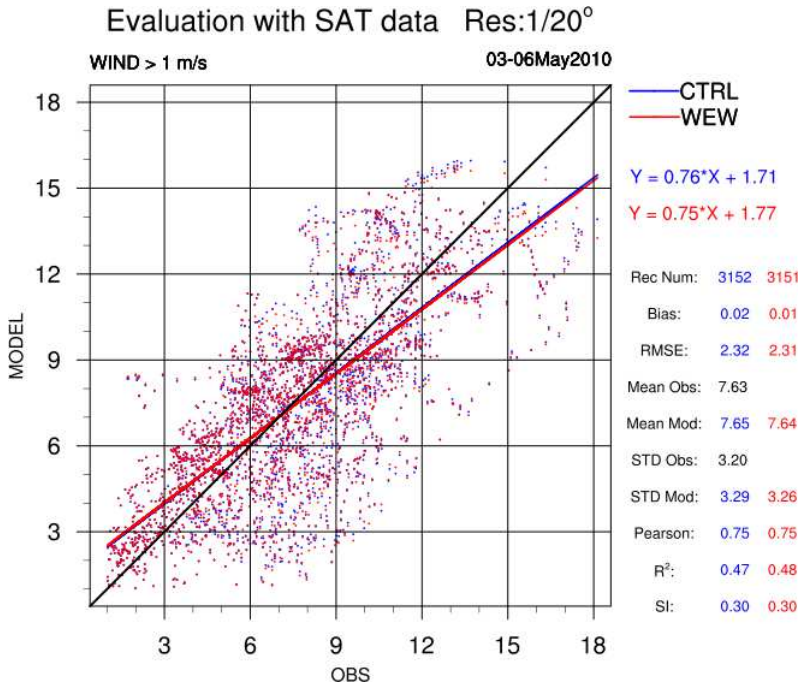

Figure VI.31: As in Figure VI.29 for the near surface wind speed exceeding 1 ms^{-1}.

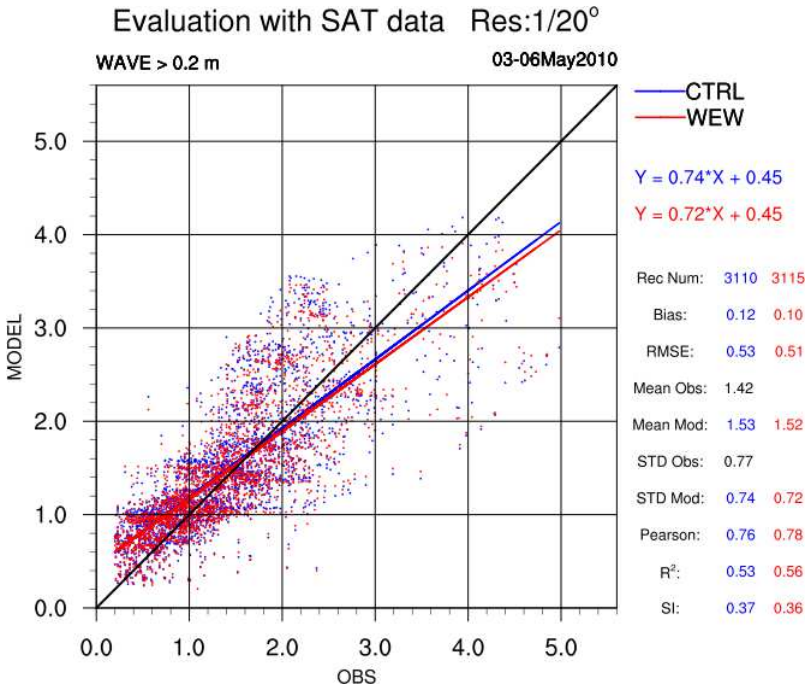

Figure VI.32: As in Figure VI.29 for the significant wave height exceeding 0.2m.

VI.2.8 Overall statistical analysis

Processing the entire data from the case studies A-D revealed an overall improvement of the statistical scores by WEW. In more details, both runs overestimate the wind speeds up to 8 ms^{-1} and underestimate above. Thus, the overall Bias error is positive, while WEW reduces it and improves the RMSE by approximately 0.5% (Figure VI.33). WEW also decreases the STD, the Mean value and improves the R^2 by 1.5%. The impact of WEW on the SWH estimation is more prominent (Figure VI.34). Despite the fact of the slightly increased underestimation, WEW substantially improves almost the entire rest indexes such as RMSE 4% and up to 4.5% for the correlation coefficients. The entire indexes have been tested as statistically significant in the 95% confidence level.

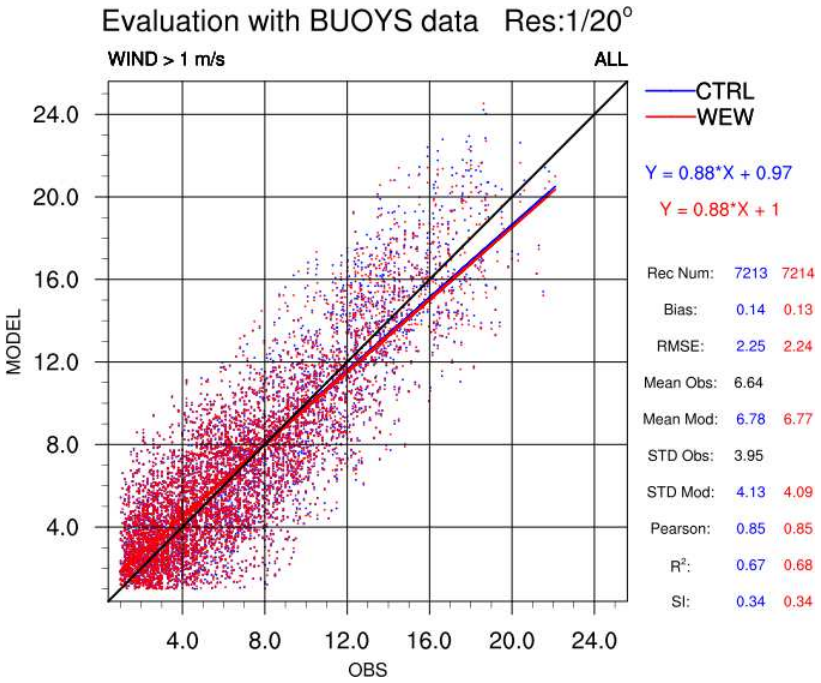

Figure VI.33: Scatter plot for near surface wind speed exceeding 1 ms^{-1}. Y-axis represents the model-estimated values and X-axis the buoys observations. CTRL and WEW evaluation results are shown in blue and red colors respectively.

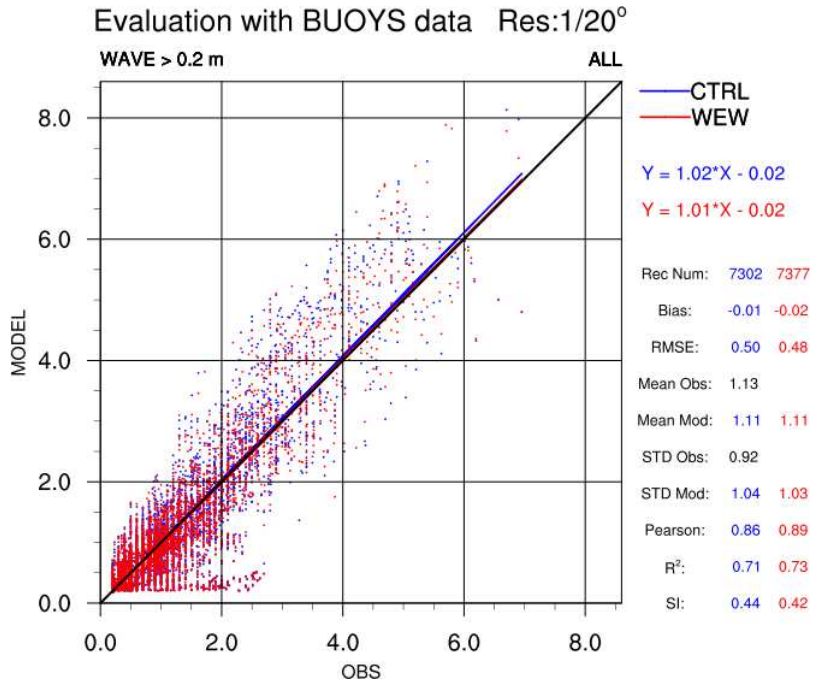

Figure VI.34: As in Figure VI.33 for the significant wave height exceeding 0.2m.

The comparison against satellite retrievals reveals a systematic underestimation of the moderate and high wind speeds (Figure VI.35). This is in agreement with the relevant wind speed scores estimated against the buoys measurements. In contrast to the buoys overestimation, the wind speed is underestimated by both runs and WEW slightly enhances the underestimation. Additionally, WEW reduces the RMSE (up to 1.4%) and provides an overall improvement for the rest indexes. The SWH is slightly overestimated by both runs and WEW offers an additional RMSE improvement by almost 5% (Figure VI.36). Its Bias score is limited to the 0.01, the STD and SI are decreased up to 6% and the correlation coefficients are increased by 2-3%.

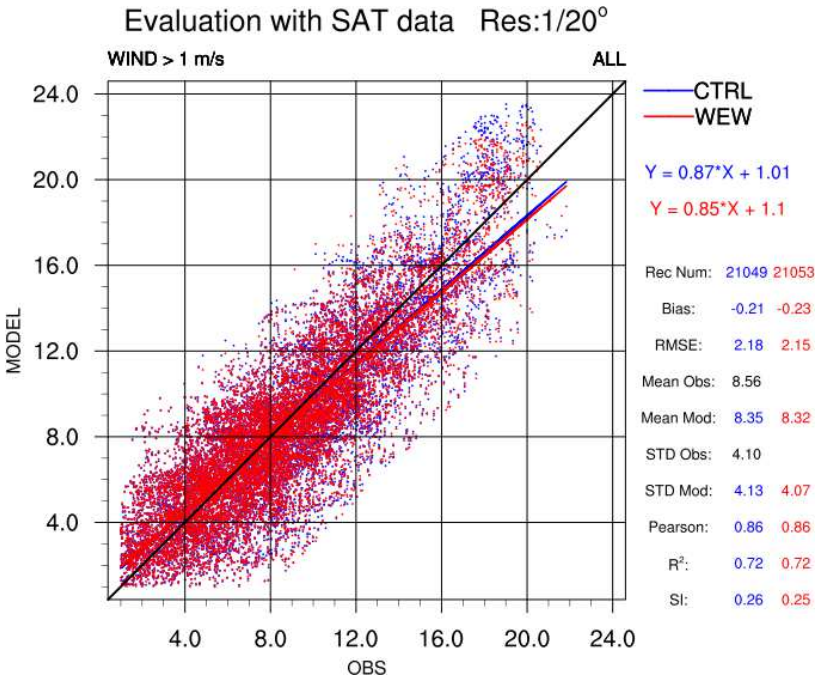

Figure VI.35: As in Figure VI.33 for the near surface wind speed exceeding 1 ms^{-1}.

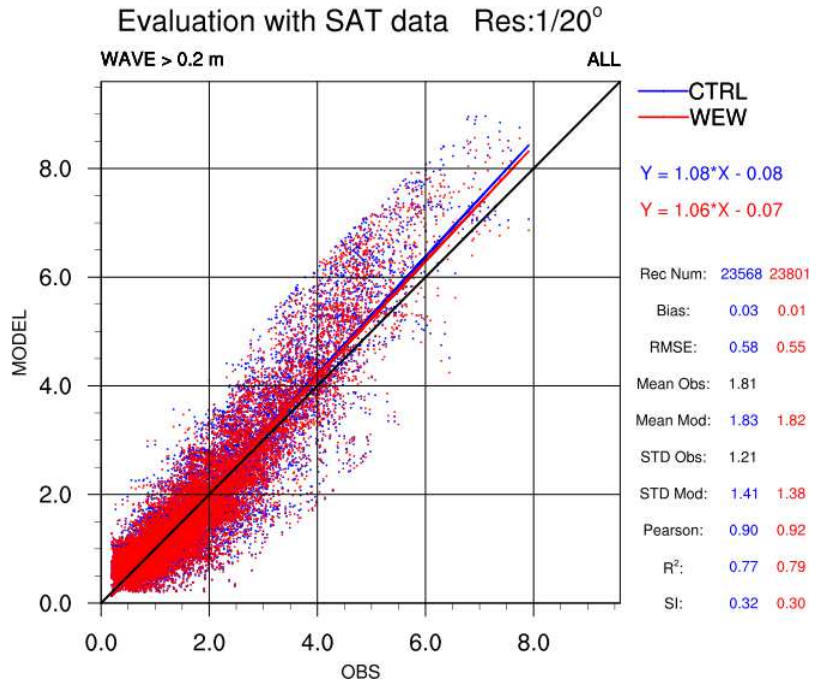

Figure VI.36: As in Figure VI.33 for the significant wave height exceeding 0.2m.

The initial version (v0.1) of WEW was configured on a coarser resolution grid of 0.10°x0.10° (Figure VI.37). Therefore the system performance is also evaluated on the coarse and fine resolutions in order to assess the impact of the horizontal resolution on the coupling and the sensitivity of the system. As it was expected, the overall scores are substantially improved in the fine resolution experiments. Moreover, WEW on coarse resolution provides marginally improved scores against the CTRL. This is an indication that the fully two-way coupling offers an overall better description for the mechanisms of the ocean surface momentum transfer, which is further improved by the finer horizontal resolution due to the adequate resolve of the additional high frequency spatiotemporal scales of motions.

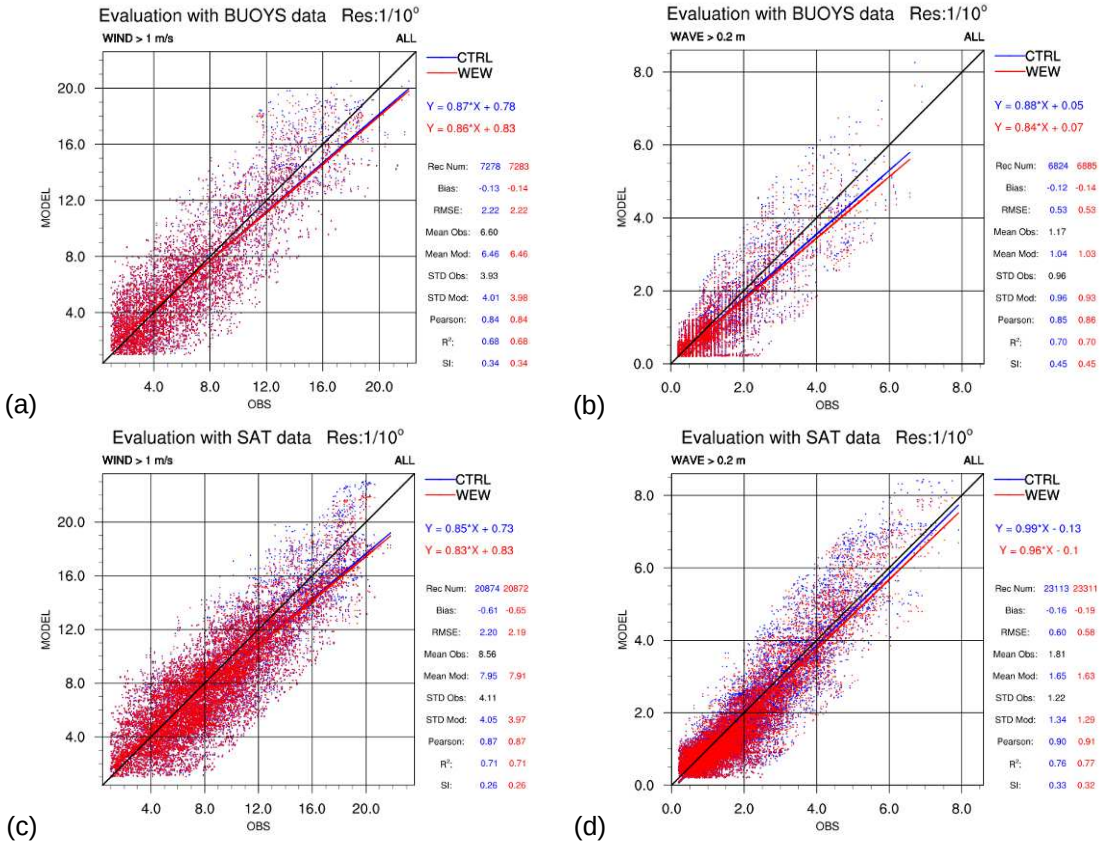

Figure VI.37: Scatter plots for the CTRL and WEW experiments on 0.10°x0.10° horizontal resolution for the near surface wind speed exceeding 1 ms^{-1} (a and c) and the significant wave height exceeding 0.2m (b and c). Y-axis represents the model-estimated values and X-axis the buoys (a and b) and satellite (c and d) records. CTRL and WEW evaluation results are shown in blue and red colors respectively.

The horizontal distribution of the wind speed and the SWH from two high-impact atmospheric and sea state cases is depicted in Figure VI.38. Winds exceeding the 22 ms^{-1} and SWH over 8m cover almost the entire Mediterranean Sea. The 2D differences between WEW and CTRL experiments reveal a systematic reduction of the wind speed and the SWH in the two-way fully coupled mode (WEW). The near cyclone-force winds increase the drag coefficient levels of the sea surface and a negative feedback is observed on the wind field near the surface. As a consequence, that negative feedback decreases the wind velocity and the SWH as well, and modifies their directions. Generally, the feedbacks ultimately create non-linear interactions between the different components and can make it difficult to access the full impact on each specific model (Warner et al., 2010).

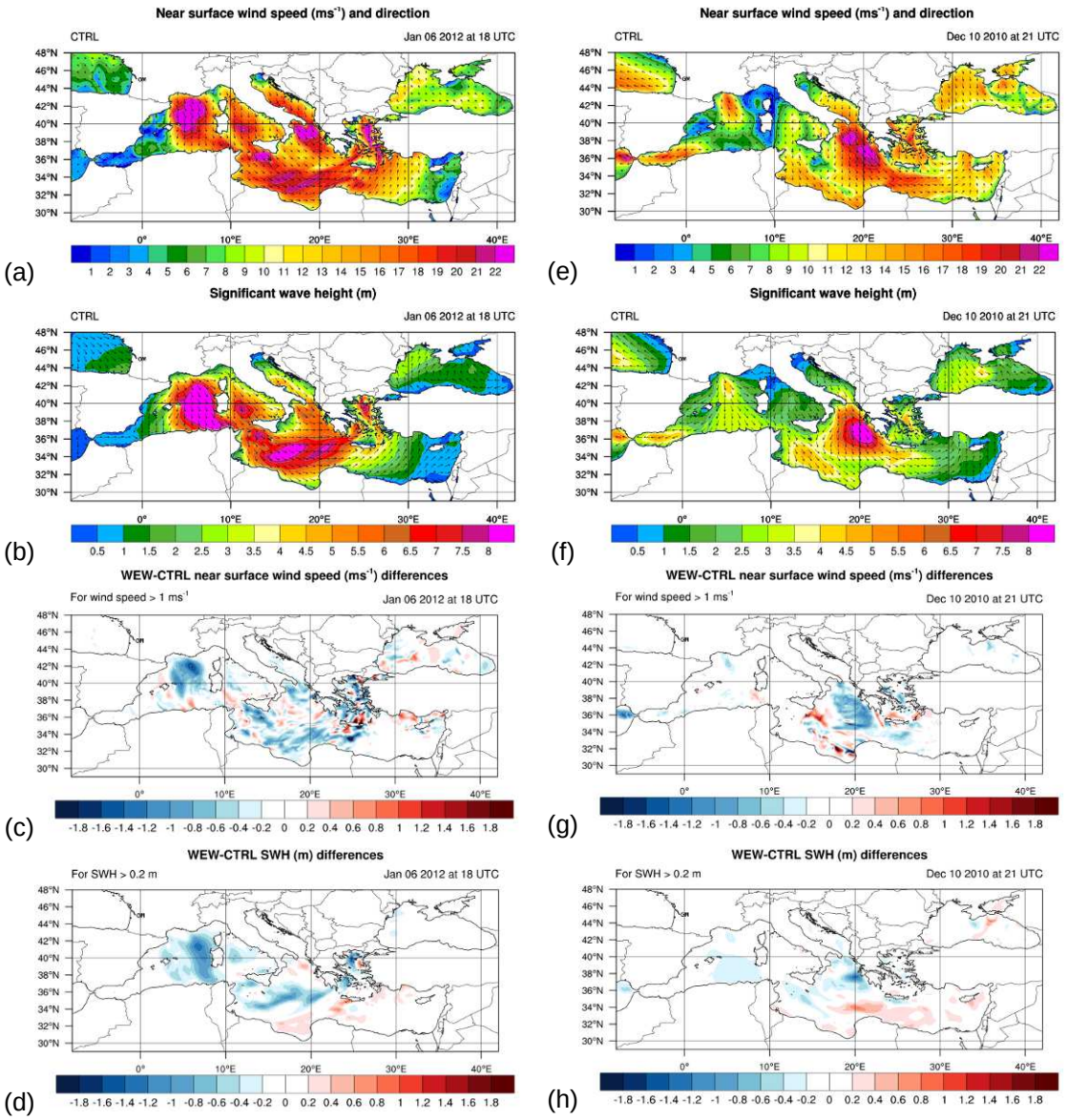

Figure VI.38: Panel of the horizontal distribution for the wind speed (a and e) and the SWH (b and f) and their differences between WEW and CTRL experiments for the wind speed (c and g) and the SWH (d and h) for two cases at January 6, 2012 at 18 UTC (a-d) and December 10, 2010 at 21 UTC (e-h).

VI.2.9 Taylor diagram

A Taylor diagram has been also applied for an overall summary of the CTRL and WEW responses. Taylor diagrams (Taylor, 2001) provide a way of graphically summarizing how closely a pattern (or a set of patterns) matches observations. The similarity between two patterns is quantified in terms of their correlation, their centered root-mean-square difference and the amplitude of their variations (represented by their standard deviations). The standard deviation of the simulated pattern is proportional to the radial distance from the origin. Also, the centered root-mean-square (RMS) difference between the simulated and observed patterns is proportional to the distance to the point on the x-axis identified as "observed".

In Figure VI.39 an overall Taylor diagram is shown for near surface wind speed and significant wave height exceeding 1 ms^{-1} and 0.2 m respectively. Blue color indicates the CTRL results and red color the WEW results. 1-2 are referred to comparison with buoys observations and 3-4 to comparison against satellite retrievals. The pair 1-3 corresponds to the wind speed and 2-4 to the SWH. From the position of dots 1 and 3, it is evidenced that the WEW simulated wind speed is characterized from better standard deviations, slightly improved RMSE and almost similar correlation against the CTRL. It

is noteworthy that the absolute scores of CTRL and WEW reveal different characteristics when they are evaluated against buoys or satellite retrievals. On the other hand, the dots 2 and 4 indicate that WEW provides reduced RMSE, improved correlation and substantially reduced standard deviation for the SWH.

In general, WEW offers an overall improvement of the simulated wind speed and the SWH which vary 1-6%. Similar conclusions have been also drawn by relevant studies (Lionello et al., 2003; Bao et al., 2000).

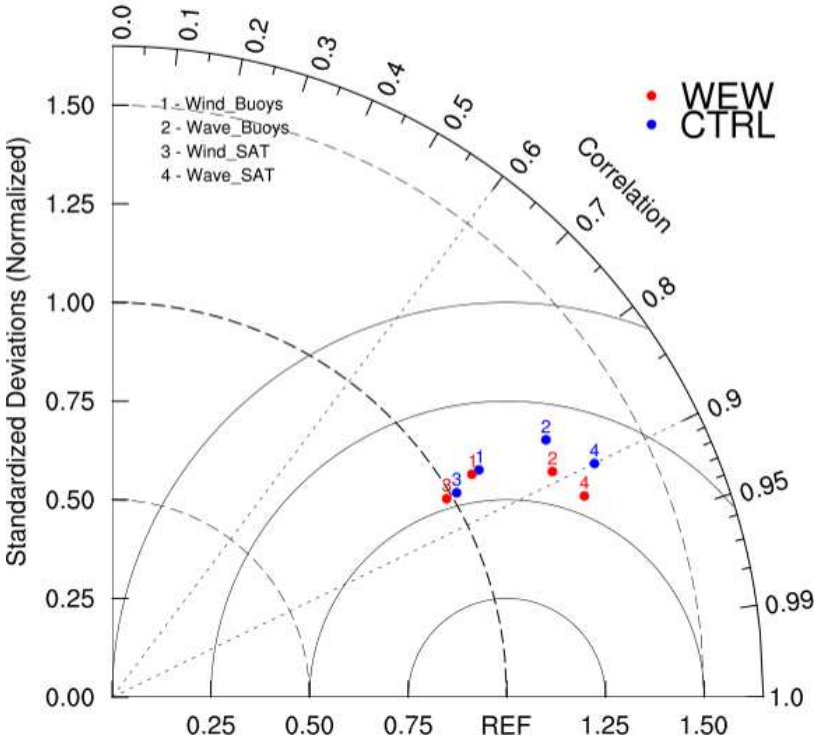

Figure VI.39: Taylor diagram for the near surface wind speed and the significant wave height exceeding 1 ms^{-1} and 0.2 m respectively. Blue color indicates the CTRL scores and red color the WEW scores. 1-2 are referred to the comparison against buoys observations and 3-4 to the comparison against satellite retrievals.

VI.2.10 Overall statistical analysis over land

Both systems have been also evaluated over land in order to assess the impact of the dynamic air-sea interaction to the atmospheric conditions over land. The systems results are compared against land surface stations records from the GTS network. The location of the almost 600 stations included in the evaluation and their spatial distribution are depicted in the Figure VI.16. The meteorological variables considered in the evaluation are: the near surface wind speed, the near surface temperature, the mean sea level pressure (MSLP) and the accumulated precipitation. The entire scores of the continuous variables are almost identical indicating an almost negligible impact of the coupling procedure on the atmospheric conditions over land (Table VI-7). The near surface temperature and the MSLP are underestimated while the near surface wind speed is overestimated by both models.

Table VI-7: Overall bias and RMSE scores at the positions of the surface meteorological stations for the near surface wind speed (ms-1), the near surface temperature (□C) and the MSL pressure (hPa).

	Wind speed		Air temperature		MSLP	
	Bias	RMSE	Bias	RMSE	Bias	RMSE
CTRL	0.57	2.42	-0.09	2.66	-0.05	1.51
WEW	0.57	2.42	-0.12	2.66	-0.04	1.50

The evaluation of the discrete variable (precipitation) has been performed for 6 predefined rainfall thresholds (0.5, 2, 4, 8, 16, and 24 mm). In general, the impact of the coupling over ocean bodies on the precipitation is almost negligible, as it is shown in following figures. However, both systems overestimate the precipitation more prominent for the medium and lower thresholds (Figure VI.40) and the various scores (ET, Heidke) are reduced with the increasing threshold (Figure VI.41-Figure VI.42). RMS errors are also gradually increased with the amount of precipitation for both systems (Figure VI.43).

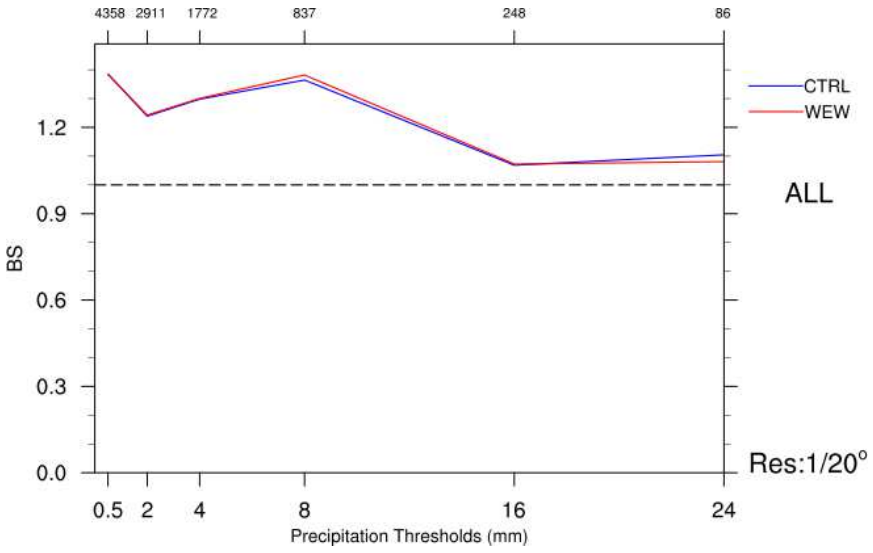

Figure VI.40: Bias scores for the CTRL (blue line) and the WEW (red line) simulations for specific precipitation thresholds. The numbers above each tick mark denote the sample for the corresponding threshold value.

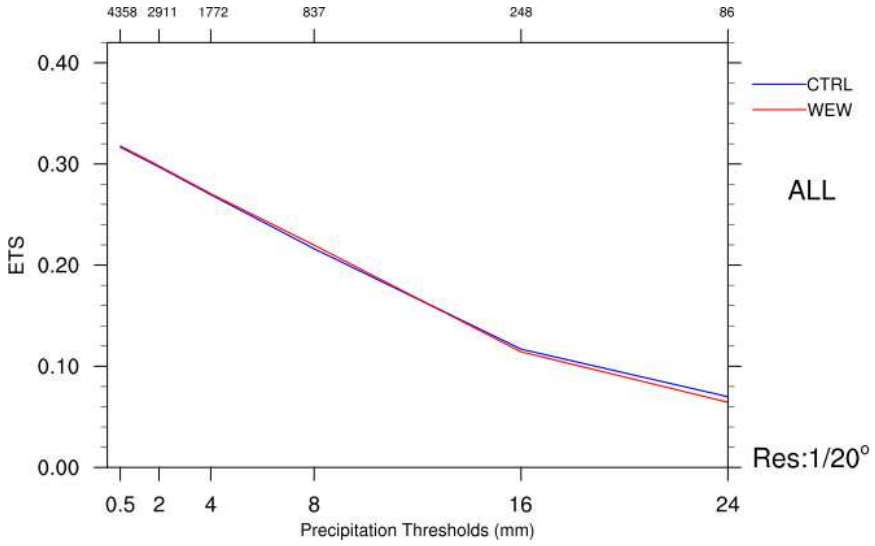

Figure VI.41: As in Fig. 2.10.1 for the equitable threat score (ETS).

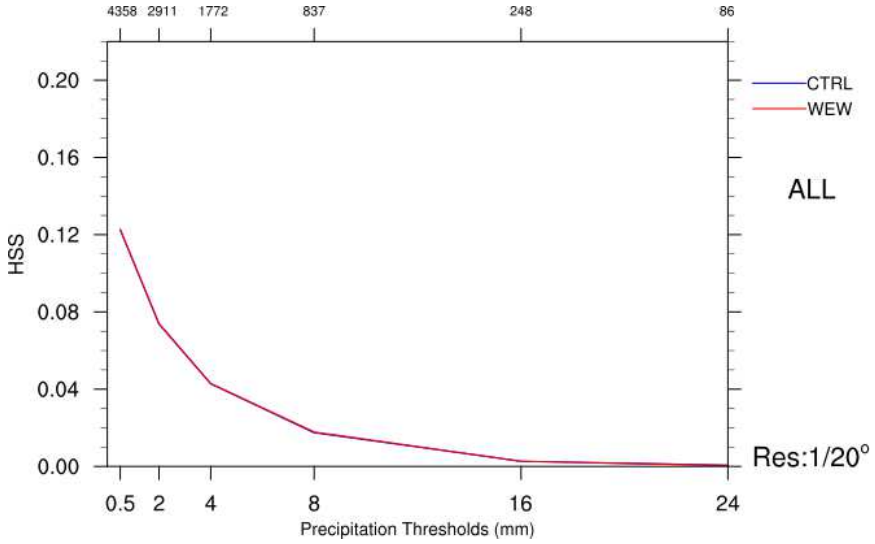

Figure VI.42: As in Fig. 2.10.1 for the Heidke skill score (HSS).

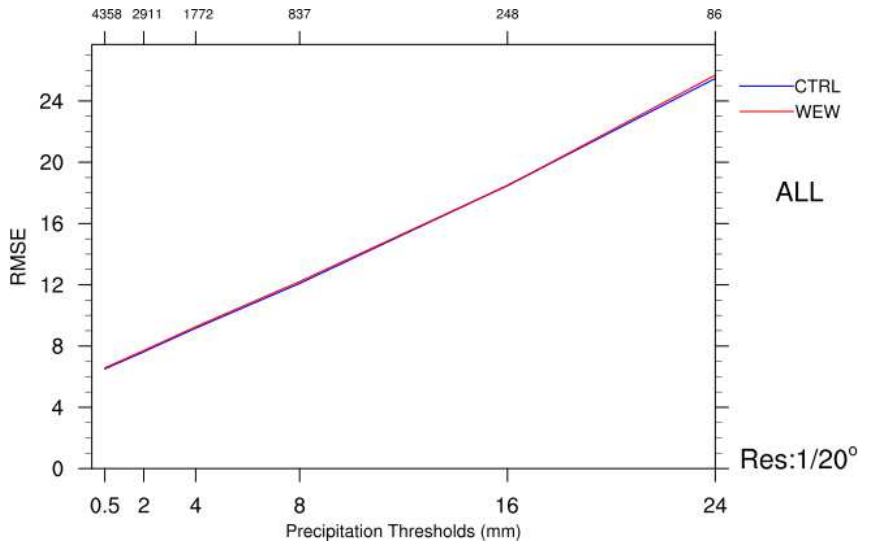

Figure VI.43: As in Fig. 2.10.1 for the root mean square error (RMSE).

VII SUMMARY AND CONCLUSIONS

The COSMO-WAM and POSEIDON/Eta-WAM two-way coupled systems have been respectively implemented and tested in the Mediterranean Sea. Both the systems use the same wave model, WAM, but different meteorological models. POSEIDON/Eta is a modified version of the Eta/NCEP model. COSMO is an extensively used product of the related consortium in Europe.

Both the implementations show, albeit at different levels, the expected reduction of the wind speeds and of the related wave heights with respect to the relative uncoupled version. However, the extent of the improvements is markedly different in the two applications. COSMO-WAM has shown substantial improvement of already high quality results in the sense that, as shown in the statistics, already low bias and RMS errors have been further reduced. As an example, wave height bias with respect to satellite measurements has been reduced at less than half of its non-coupled value. Comparison between coupled and non-coupled fields has shown macroscopic differences in the position of the centre pressure low in the most significant storm present in the two month extended test period in the Mediterranean Sea. The POSEIDON/Eta-WAM implementation has been tested on four selected events for a total of 25 days. The events were selected because of interest for the specific purpose. The performance was different from case to case, with a notable scatter, showing how the actual coupling can depend on the specific meteo-oceanographic conditions. Improvements of 0.5% in RMS error for wind were found. For wave height the coupling has led to a larger underestimate with respect to measured data, although other statistical parameters are improved. As for COSMO-WAM, significant differences were found between the coupled and uncoupled fields.

The coupling between the meteorological and wave models has been carried out with different approaches in the COSMO-WAM and POSEIDON/Eta-WAM systems. POSEIDON/Eta-WAM uses the efficient and standard Message Passing Interface (MPI) to exchange information between the two models while these are integrated in parallel without reciprocal interference. Under the parallel procedure of the Multiple Program Multiple Data (MPMD), the two tasks are carried out on parallel processors exchanging information in a direct way. Both the components keep their own executable. A similar conceptual approach has been followed for COSMO-WAM, but, in view of the expected coupling with also the ROMS circulation model, a novel coupling library, written in native FORTRAN, and been conceived and realized. This Parallel Geophysical Model Coupling Library (PGMCL) is particularly advantageous given the complicated structure of the WAM model, so conceived to increase its efficiency during massive computations. The library is efficient in terms of memory and it can be applied to any code parallelized on the base of the standard MPI interface.

As anticipated in the Introduction, the implementation of coupled meteorological-wave model systems in the Mediterranean has shown that the relevance of coupling for the final results increases with the resolution of the models. In active areas as the Mediterranean Sea this is enhanced due to the strong interactions in a transition environment between two contrasting, European and African, climates, hence with frequently strong air-sea interactions.

VIII REFERENCES

Ardhuin, F.,Jenkins, A.D., 2006: On the Interaction of Surface Waves and Upper Ocean Turbulence. J. Phys. Oceanogr., 36, 551–557. doi: http://dx.doi.org/10.1175/JPO2862.1

Babanin, A.V., 2006: On a wave-induced turbulence and a wave-mixed upper ocean layer. Geophysical Research Letters, 33, L20605, doi:10.1029/2006GL027308, 6p

Bao, J.W., Wilczak, J.M., Choi, J.K. and Kantha, L.H., 2000: Numerical simulations of air-sea interaction under high wind conditions using a coupled model: a study of hurricane development. Mon. Wea. Rev., 128, 2190–2210.

Bidlot, J., S. Abdalla, and P. Janssen, 2005: A revised formulation for ocean wave dissipation in CY25R1. Tech. Rep. Memorandum R60.9/JB/0516, Research Department,

Bretherton, F.P. and Garrett, C.J.R., 1969. Wave trains in inhomogeneous moving media. Proc. Roy. Soc., A302, 529-554.

Cavaleri, L., B.Fox-Kemper, M.Hemer, 2012, Wind waves in the coupled climate system, in publication on Bull. Amer. Meterol. Soc.

Charnock, H., 1955. Wind stress on a water surface. Q. J. Royal Meteorol. Soc. 81, 639-640.

Colle, B. A., Mass, C. F., and Westrick, K. J., 2000: MM5 precipitation verification over the Pacific northewest during 1997–1999 cool seasons, Weather Forecast., 15, 730–744.

ECMWF, 2012, IFS documentation, http://www.ecmwf.int/research/ifsdocs/

Hasselmann, K., 1961. On the non-linear energy transfer in a gravity-wave spectrum. Part 1. General theory. J. Fluid Mech., 12, 481–500.

Hasselmann, K., 1974. On the spectral dissipation of ocean waves due to whitecapping. Bound.-Layer Meteor., 6, 107-127.

Hristov, T., S. Miller, C. Friehe, “Dynamical coupling of wind and ocean waves through wave-induced air flow”, Nature, v. 422, pp. 55--58, 2003.

Janjić, Z. I., 1994: The step-mountain eta coordinate model: further developments of the convection, viscous sublayer, and turbulence closure schemes. Mon. Wea. Rev., 122, 927–945. doi: http://dx.doi.org/10.1175/1520-0493(1994)122<0927:TSMECM>2.0.CO;2.

Janjic, Z. I., Gerrity J. P. Jr., and Nickovic, S., 2001: An Alternative Approach to Nonhydrostatic Modeling, Mon. Wea. Rev., 129, 1164-1178.

Janssen, P.A.E.M., 1982. Quasilinear approximation for the spectrum of wind-generated water waves. J. Fluid Mech. 117, 493-506.

Janssen, P.A.E.M., 1989. Wave-induced stress and the drag of air flow over sea waves. J. Phys. Oceanogr. 19, 745-754.

Janssen, P.A.E.M., 1991. Quasi-linear theory of wind wave generation applied to wave forecasting. J. Phys. Oceanogr. 21, 1631-1642.

Janssen, P. A. E. M., O. Saetra, C. Wettre, H. Hersbach , 2004, Impact of the sea state on the atmosphere and ocean, Annales Hydrographiques, Vol. 6e série, vol. 3, No. 772. (2004)

Janssen. P.A.E.M. 2010, Ocean wave effects on the daily cycle in STT, ECMWF, Technical Memorandum.

Kallos, G., Nickovic, S., Papadopoulos, A., et al., 1997: The regional weather forecasting system SKIRON: An overview, in: Proceedings of the Symposium on Regional Weather Prediction on Parallel Computer Environments, Athens, Greece, 15–17 October 1997, 109-122.

Katsafados, P., Papadopoulos, A., Varlas, G., and Korres, G., 2014: The coupled atmosphere-ocean wave modeling system WEW. 12th International Conference on Meteorology, Climatology and Atmospheric Physics (COMECAP 2014), University of Crete, Heraklion, Crete, Greece, 28-31 May 2014.

Katsaros, K.B., S.D. Smith and W.A. Oost, 1987. HEXOS - Humidity Exchange Over the Sea. A program for research on water-vapor and droplet fluxes from sea to air at moderate to high wind speeds. Bull. Amer. Meteor. Soc. 68, 466-476.

Keller, J.B., 1958. Surface waves on water on non-uniform depth. Journal of Fluid Mechanics 4, 607–614.

Komen, G.J., L. Cavaleri, M. Donelan, K. Hasselmann, S. Hasselmann, and P.A.E.M. Janssen, 1994. Dynamics and Modelling of Ocean Waves, Cambridge University Press, Cambridge.

Korres, G., Nittis, K., Perivoliotis, L., Tsiaras, K., Papadopoulos, A., Triantafyllou, G., & Hoteit, I., 2010: Forecasting the Aegean Sea hydrodynamics within the POSEIDON-II operational system. Journal of Operational Oceanography, 3(1), 37-49.

Korres, G., Papadopoulos, A., Katsafados, P., Ballas, D., Perivoliotis, L., and Nittis, K., 2011: A 2-year intercomparison of the WAM-Cycle4 and the WAVEWATCH-III wave models implemented within the Mediterranean Sea..Mediterranean Marine Science, 12(1), 129-152.

Lionello, P., G. Martucci, and M. Zampieri, 2003: Implementation of a coupled atmosphere-wave-ocean model in the Mediterranean Sea: Sensitivity of the short time scale evolution to the air-sea coupling mechanisms, Global Atmos. Ocean Syst., 9, 65 – 95.

Makin, K., 2005: A note on the drag of the sea surface at hurricane winds. Bound. Lay. Meteor. 115.1: 169-176.

Mass, C. F., Ovens, D., Westrick, K. J., and Colle, B. A., 2002: Does increasing horizontal resolution produce more skillful forecasts?, B. Am. Meteorol. Soc., 83, 407-430.

Mesinger, F., 1996: Improvements in quantitative precipitation forecasts with the Eta regional model at the National Centers for Environmental Prediction: The 48-km upgrade, B. Am. Meteorol. Soc., 77, 2637–2649.

Mesinger, F., Janjic, Z.I., Nickovic, S., Gavrilov, D., and Deaven, D.G., 1988: The step-mountain coordinate: Model description and performance for cases of Alpine lee cyclogenesis and for a case of an Appalachian redevelopment, Mon. Wea. Rev., 116, 1493-1518.

Miles, J.W., 1957. On the generation of surface waves by shear flows. J. Fluid Mech. 3, 185-204.

Monbaliu, J., Hargreaves, R., Albiach, J., Luo, W., Sclavo M., and Günther, H., 2000: The spectral wave model, WAM, adapted for applications with high spatial resolution. Coastal Engineering, 41, 41-62.

NCL (The NCAR Command Language) (Version 6.1.2) [Software], 2013: Boulder, Colorado: UCAR/NCAR/CISL/VETS. http://dx.doi.org/10.5065/D6WD3XH5.

Nickovic, S., Kallos, G., Papadopoulos A., and Kakaliagou, O., 2001: A model for prediction of desert dust cycle in the atmosphere, J. Geophophys. Res., 106, 18113-18129.

Papadopoulos, A., Katsafados, P., Kallos, G., Nickovic, S., 2002: The weather forecasting system for POSEIDON-An overview, Global Atmos. Ocean Syst. 8 (2-3): 219-237.

Papadopoulos, A., and Katsafados, P., 2009: Verification of operational weather forecasts from the POSEIDON system across Eastern Mediterranean. Nat. Haz. Eart. Sys. Sci. 9(4): 1299-1306.

Phillips, O.M., 1957. On the generation of surface waves by turbulent wind. J. Fluid Mech., 2, 417-445.

Taylor, K. E., 2001: Summarizing multiple aspects of model performance in a single diagram. Journal of Geophysical Research: Atmospheres (1984–2012), 106(D7), 7183-7192.

Troitskaya, Y. I., O. Druzhinin, and S. Zilitinkevich (2012), Direct numerical simulation of a turbulent wind over a wavy water surface, J. Geophys. Res., doi:10.1029/2011JC007789, in press.

Varlas, G., Papadopoulos A., Korres G., and Katsafados P., 2014: Modeling the air-sea wave interaction processes in an explosive cyclone over the Mediterranean Sea. 12th International Conference on Meteorology, Climatology and Atmospheric Physics (COMECAP 2014), University of Crete, Heraklion, Crete, Greece, 28-31 May 2014.

WAMDI group: S. Hasselmann, K. Hasselmann, E. Bauer, P.A.E.M. Janssen, G.J. Komen, L. Bertotti, P. Lionello, A. Guillaume, V.C. Cardone, J.A. Greenwood, M. Reistad, L. Zambresky and J.A. Ewing, 1988. The WAM model - a third generation ocean wave prediction model. J. Phys. Oceanogr. 18, 1775-1810.

Warner, J. C., Armstrong, B., He, R., and Zambon, J. B.: Development of a coupled ocean-atmosphere-wave-sediment transport (COAWST) modeling system. Ocean modelling, 35(3), 230-244, 2010.

Wilks, S., 1995: Statistical Methods in the Atmospheric Sciences, Academic Press, 233-242.

IX ANNEX A

IX.1 Verification Measures (HCMR)

The formulas of the evaluation indexes for N measurements, where M_i and O_i are the model-estimated and the observed values respectively (Wilks, 1995), are shown below:

$$MeanObs = \frac{1}{N}\sum_{i=1}^{N} O_i \quad (32)$$

$$MeanMod = \frac{1}{N}\sum_{i=1}^{N} M_i \quad (33)$$

$$STDObs = \sqrt{\frac{1}{N}\sum_{i=1}^{N} (O_i - \overline{O})^2} \quad (34)$$

$$STDMod = \sqrt{\frac{1}{N}\sum_{i=1}^{N} (M_i - \overline{M})^2} \quad (35)$$

$$Bias = \frac{1}{N}\sum_{i=1}^{N} (M_i - O_i) \quad (36)$$

$$RMSE = \sqrt{\frac{1}{N}\sum_{i=1}^{N} (M_i - O_i)^2} \quad (37)$$

$$Pearson = \frac{\sum_{i=1}^{N} (O_i - \overline{O})(M_i - \overline{M})}{\sqrt{\sum_{i=1}^{N} (O_i - \overline{O})^2}\sqrt{\sum_{i=1}^{N} (M_i - \overline{M})^2}} \quad (38)$$

$$R^2 = 1 - \frac{\sum_{i=1}^{N} (M_i - O_i)^2}{\sqrt{\sum_{i=1}^{N} (O_i - \overline{O})^2}} \quad (39)$$

$$SI = N\frac{\sqrt{\frac{1}{N}\sum_{i=1}^{N} (M_i - O_i)^2}}{\sum_{i=1}^{N} O_i} = \frac{RMSE}{MeanObs} \quad (40)$$

IX.2 Verification Measures (CNMCA)

Suppose that we have N measurement x'_i and corresponding N modelled values x_i. Then the mean error of the model, or bias, is defined as

$$ME = \frac{1}{N}\sum_{i=1}^{N} x'_i - x_i \tag{41}$$

The absolute error of the model is defined as

$$AE = \frac{1}{N}\sum_{i=1}^{N} | x'_i - x_i | \tag{42}$$

The Root Mean Square Error of the model is defined

$$RMSE = \sqrt{\frac{1}{N}\sum \left(x'_i - x_i\right)^2} \tag{43}$$

The Centered Root Mean Square Error is defined as

$$CRMSE = \sqrt{RMSE^2 - ME^2} \tag{44}$$

The Correlation is defined as

$$Corr = \frac{\sum_{i=1}^{N}\left(x'_i - m(x')\right)\left(x_i - m(x)\right)}{\sqrt{\sum_{i=1}^{N}\left(x'_i - m(x')\right)^2 \sum_{i=1}^{N}\left(x_i - m(x)\right)^2}} \tag{45}$$

with

$$m(x) = \frac{1}{N}\sum_{i=1}^{N} x_i \tag{46}$$

The Scatter Index is defined as

$$SI = \frac{RMSE}{m(x)} \tag{47}$$

The Centered Scatter Index is defined as

$$CSI = \frac{CRMSE}{m(x)} \tag{48}$$